This article has been accepted for publication in a future issue of this journal, but has not been fully edited. Content may change prior to final publication. Citation information: DOI 10.1109/JESTPE.2021.3077203, IEEE Journal of Emerging and Selected Topics in Power Electronics

Analytical Expressions for Inductances of 3D Air Core Inductors for Integrated Power Supply

Chandra Shetty, *Student Member, IEEE,* Youssef Kandeel, *Student Member, IEEE,* Liang Ye, Séamus O'Driscoll, Paul McCloskey, Maeve Duffy, *Senior Member, IEEE,* and Cian O'Mathuna, *Fellow, IEEE*

***Abstract*—This work presents analytical expressions for the DC inductance of 3D air core inductors with circular cross section pillars (CCSP) and rectangular cross section pillars (RCSP). We consider the following four types of inductor structures: (1) a toroid with CCSP; (2) a toroid with RCSP; (3) a solenoid with RCSP; and (4) a solenoid with CCSP. For each type, a unique analytical model is developed for obtaining DC inductance. High frequency (1-100 MHz) effects on inductance are also discussed. The inductance values predicted by the proposed analytical models of the first three types of inductor structures are in an acceptable agreement with numerical Finite Element Analysis (FEA) solutions, where the maximum difference is 7.3%. Also, our analytical model for the fourth type inductor reduces the error, when correlated with FEA inductance value, up to $6\times$ compared to previously published models. A comparison of results using proposed analytical expressions with published measured values as well as our measurement data demonstrates error ranging from 0.5 to 16.2%, while conventional formulae show errors of up to 143%. The results of the proposed models could serve as a good initial estimate for power supply on chip (PwrSoC) and power supply in package (PSiP) applications.**

***Index Terms*—Inductance model, 3D solenoid inductor, 3D toroidal inductor, self-inductance, mutual inductance, partial inductance, loop inductance, through silicon via (TSV), air core, power supply on chip (PwrSoC), power supply in package (PSiP).**

NOMENCLATURE

μ_r	Relative permeability.
μ_o	Permeability of free space ($4\pi \times 10^{-7}\ H/m$).
H	Magnetic field strength.
f	Frequency.
ρ	Radius of circular pillar.
N	Number of turns.
θ	Angle between any two turns.
R_i	Inner radius of the toroidal inductor.
R_o	Outer radius of the toroidal inductor.
l_p	Length of copper pillar.
α_p	Width of the copper pillar.
β_p	Height of the copper pillar.
α_i	Width of the interconnect.
β_i	Height of the interconnect.
L_{circ}	Self-inductance of a circular cross sectiion conductor.
L_{rect}	Self-inductance of a rectangular cross section conductor.
L_{RECT_1}	Self-inductance of a rectangular loop with non-uniform rectangular cross section conductors.
L_{RECT_2}	Self-inductance of a rectangular loop with uniform rectangular cross section conductors.
L_{sq_1}	Self-inductance of a square loop with uniform rectangular cross section conductors.
L_{sq_2}	Self-inductance of a square loop with square cross section conductors.
L_{ip}	Self-inductance of inner pillar.
L_{op}	Self-inductance of outer pillar.
L_{ti}	Self-inductance of the top interconnect.
L_{bi}	Self-inductance of the bottom interconnect.
$\begin{cases} L_{i\_ST} \\ i = 1, 2, \\ 3, 4 \end{cases}$	Self-inductance of a single turn of *type 1*,*type 2*, *type 3*, and *type 4* inductors, respectively.
$L_{3\_ST(rect)}$	Self-inductance of a single turn (rectangular shape with rectangular cross section conductors) of *type 3* inductor.
$L_{3\_ST(sq)}$	Self-inductance of a single turn (square shape with square cross section conductors) of *type 3* inductor.
L_{1_e}	Total inductance (self and mutual inductances) of *type 1* inductor with even turns.
L_{1_o}	Total inductance of *type 1* inductor with odd turns.
L_3	Total inductance of *type 3* inductor.
L_{in}	Internal inductance of a conductor.
L_{ex}	External inductance of a conductor.
M_{par}	Mutual inductance between parallel conductors.
M_{lm_1}	Mutual inductance between two conductors at an angle.
M_{lm_2}	Mutual inductance between two skewed and displaced conductors.
M_{rect}	Mutual inductance between two filamentary parallel rectangles.
M_{sq}	Mutual inductance between two filamentary parallel squares.
M_θ	Mutual inductance between any two turns at an

This work is funded by SFI under the project 15/IA/3180 (ADEPT). (*Corresponding authors: Chandra Shetty and Cian O'Mathuna.*)

The paper has not been presented at a conference or submitted elsewhere previously.

C. Shetty, L. Ye, S. O'Driscoll, P .McCloskey and C. O'Mathuna are with the Microsystems Centre, Tyndall National Institute, University College Cork, Cork T12R5CP, Ireland (e-mail: chandra.shetty@tyndall.ie; liang.ye@tyndall.ie; seamus.odriscoll@tyndall.ie; paul.mccloskey@tyndall.ie; cian.omathuna@tyndall.ie).

Y.kandeel and M. Duffy are with the Electrical and Electronic Engineering, National University of Ireland, Galway, Ireland (e-mail: Y.KANDEEL1@nuigalway.ie; maeve.duffy@nuigalway.ie).

This article has been accepted for publication in a future issue of this journal, but has not been fully edited. Content may change prior to final publication. Citation information: DOI 10.1109/JESTPE.2021.3077203, IEEE Journal of Emerging and Selected Topics in Power Electronics

angle.

M_{ip}	Mutual inductance between inner pillars.
M_{op}	Mutual inductance between outer pillars.
M_{bi}	Mutual inductance between bottom interconnects.
M_{ti}	Mutual inductance between top interconnects.
M_{io_ST}	Mutual inductance between inner and outer pillars of a single turn.
M_{io_TT}	Mutual inductance between inner and outer pillars of two turns.
M_{bt_ST}	Mutual inductance between the bottom and top interconnects of a single turn.
M_{bt_TT}	Mutual inductance between the bottom and top interconnects of two turns.
M_{1_e}	Net mutual inductance of the *type 1* inductor with even turns.
M_{1_o}	Net mutual inductance of the *type 1* inductor with odd turns.
M_3	Net mutual inductance of *type 3* inductor.
$M_{s(rect)}$	Mutual inductance between two rectangular shape turns of the *type 3* inductor with spacing *s*.
$M_{s(sq)}$	Mutual inductance between two square shape turns of the *type 3* inductor with spacing *s*.

I. Introduction

INDUCTORS are essential components in power supplies. Increasingly, point-of-load (POL) power delivery is now the primary issue across all market sections, such as battery-powered portable electronic systems, including laptops, smartphones, tablets, etc [1]. With increasing performance and decreasing footprint, there is a rising demand for on-chip three dimensional (3D) inductors [2], [3]. Micro inductors are used in on-chip voltage regulators, radio-frequency (RF) circuits, micro sensors, micro actuators, power MEMS devices, etc. The benefits of 3D inductors can be extended to such applications. On-chip inductors are classified either as magnetic core inductors or air core inductors. Although magnetic core inductors can achieve high inductance density, the loss associated can limit operation at very high frequencies. The presence of core will reduce the Q-factor of the inductor unless the core is laminated and low loss magnetic cores are used; also, it is difficult to induce anisotropy in magnetic cores [4]. Another challenge is the integration of the magnetic core for the toroidal inductors [5]. On the other hand, air core inductors have limited inductance density, but have no core loss, which enables air core inductors to be used in the higher-frequency range (>10 MHz) [6]–[8]. High frequency operation reduces the inductance requirement of power converters; however, at the same time it introduces switching losses. Resonant converters employ soft switching to reduce switching losses. As a consequence, air core inductors find good application in resonant converters [9].

In principle, the modelling of inductors is more complicated than the modelling of other components of electrical engineering such as resistors. This is particularly true of air-core inductors, where the variation in coupling between different pairs of turns is significant due to the absence of a core. Therefore, simplified analytical equations for the inductance of inductors with magnetic cores that are based on an assumption of ideal coupling are not accurate. Simulators such as ANSYS Q3D and ANSYS Maxwell can be used to obtain an accurate numerical solution for the inductance of 3D inductors. However, simulators demand huge computation time and are also expensive to license. Conventional analytical expressions for the inductance of toroidal and solenoidal inductors are not suitable for 3D inductors (section II offers a comprehensive explanation); typical errors are more than 20%. Hence, there is motivation to derive better analytical models for the inductance of 3D inductors.

For an effective research, we should put as much emphasis on analytical modelling as we do on experimental research. Analytical methods can evaluate the quality of the experimental data. Even though there are numerous published works on the fabrication of 3D toroidal inductors [10], [11], little or no attention has been given to validating experimental data with analytical expressions for inductance. The same holds true for fabricated 3D solenoid inductors [12], [13]. This may be due to the fact that little progress or no attempt towards the development of analytical models for the inductance of 3D inductors has been made. In previous works [14], [15], considerable effort has been made to develop an analytical expression for the inductance of 3D solenoid inductors with CCSP. These analytical models are based on the self-inductances of individual conductors and the mutual inductance between any two conductors. In [14], the analytical model introduces large error, up to 11.67% when compared with FEM simulated inductance value, due to approximations, which are described as follows: (1) rectangular conductors are approximated as circular conductors, and (2) skewed and displaced conductors are treated as parallel conductors. On the other hand, [15] proposes a better analytical model compared to [14], maximum error is around 3.6%. The disadvantage of this model is the involvement of the computation of mutual inductances of a large number of conductor pairs for the estimation of the net mutual inductance (mutual inductances of all the turn pairs), which contributes to error. We have developed a new analytical model for the inductance of such inductor structures in section III. Our model directly computes the mutual inductance between any two turns, without the requirement of the calculation of mutual inductances of conductor pairs. As a result, the proposed model requires a lower number of pairs of turns than pairs of conductors for the estimation of the net mutual inductance. Hence, our model achieves higher accuracy compared to the analytical model from [15]; maximum error exhibited by our model is 1.78%. More details on the reason for the improved accuracy is dealt in section IV. As far as a toroid with CCSP, a toroid with RCSP and a solenoid with RCSP are concerned, this is the first attempt, based on the literature survey, for developing an analytical model.

In this work, we have developed new analytical models for the inductances of 3D inductors such as the solenoid and the toroid. Fig. 1(a)-(d) show the parameterized physical structures for a toroidal inductor with CCSP, a toroidal inductor with RCSP, a solenoidal inductor with RCSP, and a solenoidal in-

ductor with CCSP, respectively. Our model treat the inductors either as (1) a group of loop currents, where the number of loops equal to the number of turns, or (2) a group of piecewise current sources: each segment of the 3D inductor, which is formed by a number of piecewise-straight conductor segments, considered as a current source. The proposed analytical models (which represents physical phenomena) are a set of linear and nonlinear equations: the basic equations are borrowed from the previously published works and the applied equations, relating the partial and loop inductances (self and mutual) to the inductances of multi turn loops such as the solenoid and the toroid, are introduced on our own. Also, the proposed formulas are tested with our measurement data as well as previously published measurements.

The rest of this paper is organized as follows. The basic equations for self and mutual inductances are introduced in section II. In section III, analytical models for four different types of inductors are presented. In section IV, the accuracy of the proposed models is evaluated with electromagnetic field simulation solution (ANSYS Maxwell and ANSYS Q3D), and measurement data from this and previous works. Also, the accuracy of the proposed analytical models is compared with that of previously published models. Significance, application and performance of all four types is presented in section V. High frequency effects on inductance are discussed in section VI. Section VII draws some conclusions.

II. BACKGROUND THEORY

This section is dedicated to reintroducing all the associated formulas for self and mutual inductances of straight conductors as well as turn geometries composed of straight conductors, such as rectangular and square loops, from the previously published literature [16]–[19]. The formulas are based on the concept of a partial inductance, which has been reviewed in [20], [21]. The conventional, self-inductance, and mutual inductance formulas are presented in Appendix A, Appendix B, and Appendix C, respectively. The relative permeability (μ_r) is assumed to be unity in all the formulas.

As mentioned in the introductory section, this work focus on the development of the analytical models for 3D toroidal and solenoidal inductors as existing conventional models are not suitable to compute the inductance of 3D micro inductors. The conventional formulas for the inductance of toroidal and solenoidal inductors, given by (A.1) and (A.2) (refer to the Appendix A), respectively, are derived with the following assumptions: (1) the coil length, l, is greater than the radius (r) of the core, $l >> r$ for a solenoid, (2) the H-field is confined within the core and is in the circumferential direction for a toroid, (3) the relative permeability of the core is very large, $\mu_r >> 1$, and (4) the system exhibits cylindrical symmetry. Since 3D microfabricated air-core inductors do not possess these properties, there is a necessity to derive alternative expressions.

3D inductors can either be embedded within the substrate (in-chip or substrate embedded inductors) [11] or fabricated on top of the substrate (on-chip or on-substrate inductors) [22]. In both categories, the inductor consists of a combination of vertical conductors and interconnecting conductors. In the former category, vertical conductors are sometimes formed as through-silicon-vias (TSVs) [23], [24]. There is one main distinction, which is necessary to consider for developing an analytical model, for these two categories: for substrate-embedded inductors, the height of the vertical conductor is equal to the height of the substrate, whereas for on-substrate inductors it is equal to the photoresist height. Throughout this paper, we use the term copper pillar (or simply pillar) in lieu of vertical winding, vertical conductor or TSV, which are used in the literature. By the same token, we use the term interconnect for radial conductor, copper slab, redistribution layer (RDL) or metal track.

The solenoid and toroidal 3D inductors can be constructed with conductors of circular or rectangular cross section, as shown in Fig.1. All the four inductor formats we considered comprise of straight conductors. The total inductance of the complete inductor structure is the summation of the self-inductances of all straight conductors connected in series to form a turn and the mutual inductances between all resulting pairs of turns.

A. Self-Inductance Formulas

Here, we introduce the self-inductance of different types of geometries such as straight conductors with circular and rectangular cross sections and a rectangular loop composed of square cross section or rectangular cross section conductors.

1) Self-inductance of a straight conductor: The self-inductance of a straight conductor of length *l*, with a circular cross section of radius ρ is given by (B.1) [16].

Similarly, the self-inductance of a conductor of length *l* and rectangular cross section $\alpha \times \beta$ is given by (B.2) [19].

2) Self-inductance of a rectangular loop [16]: The self-inductance of a rectangular loop, having length a and breadth b, composed of four rectangular cross section conductors of sides α and β can be calculated from (B.3).

In (B.3), it is assumed that the cros section of the rectangular loop is non-uniform (i.e., conductors along the length a and the breadth b have cross section $\alpha_a \times \beta_a$ and $\alpha_b \times \beta_b$, respectively). If all four conductors of the rectangular loop have the same cross section, that is, $(\alpha + \beta)_a = (\alpha + \beta)_b$, the formula (B.3) reduces to (B.4).

For a square loop, *a* = *b*, (B.4) simplifies to (B.5). If α = β, the section of the conductor is a square, (B.5) is further simplified to (B.6).

B. Mutual-Inductance Formulas

Here, we reproduce mutual inductances of different types of geometries such as parallel straight conductors, conductors at an angle, skewed and displaced conductors.

1) Mutual inductance between two parallel conductors [16]: To calculate the mutual inductance between two parallel conductors of length l and separation D, we can use (C.1), which is valid for both circular as well as rectangular cross section conductors. Here, D is the distance between the centers of the conductors.

This article has been accepted for publication in a future issue of this journal, but has not been fully edited. Content may change prior to final publication. Citation information: DOI 10.1109/JESTPE.2021.3077203, IEEE Journal of Emerging and Selected Topics in Power Electronics

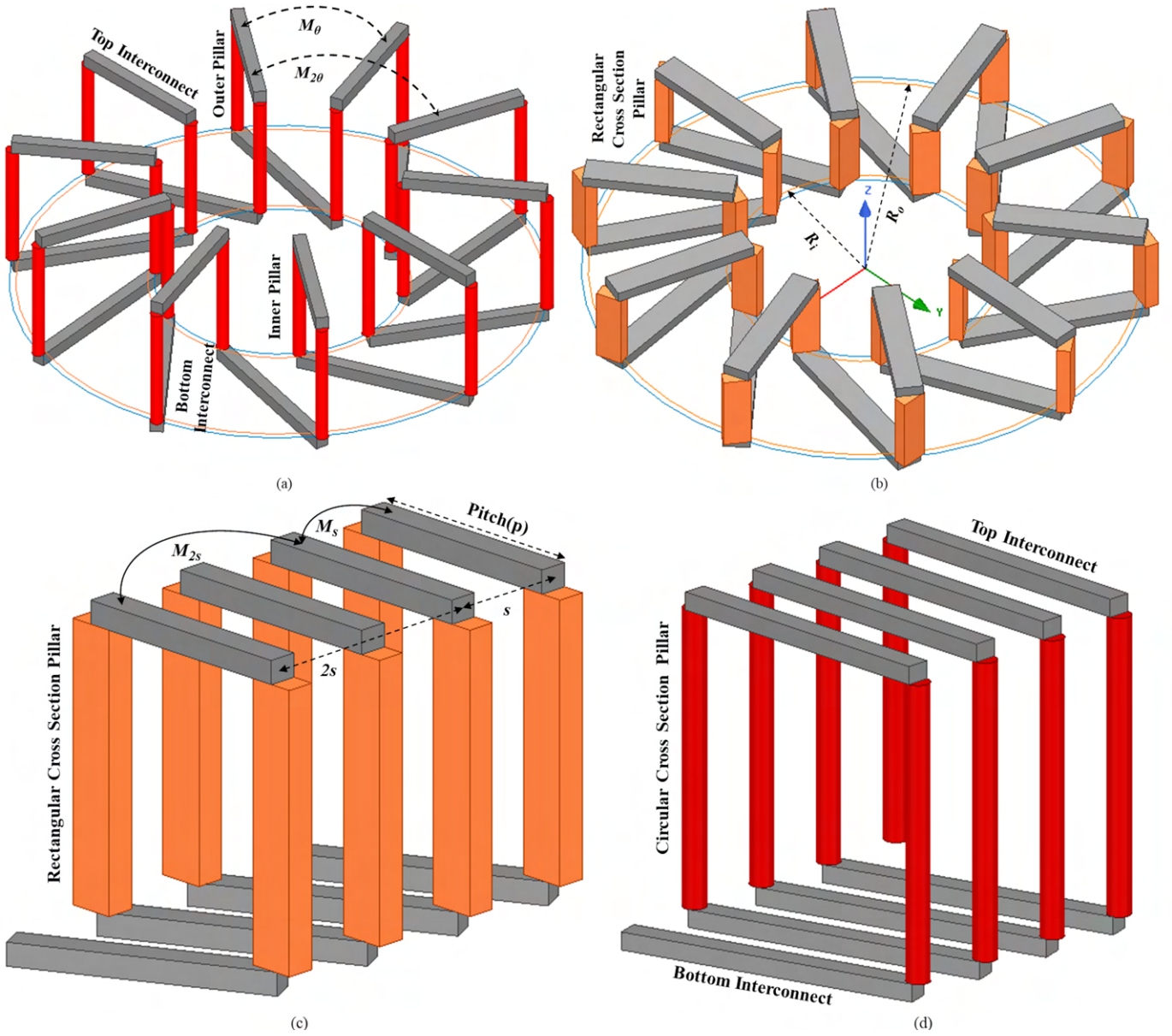

Fig. 1. 3D parameterized mechanical drawings of inductor structures: (a) toroid with CCSP (b) toroid with RCSP (c) solenoid with RCSP, (d) solenoid with CCSP.

2) Mutual inductance between two conductors at an angle [17], [18]: Fig. 2 shows two conductors having lengths l and m, and placed at an angle θ in the same plane. When the lengths l and m are extended to the point of intersection, extension lengths μ and ν will be generated. The mutual inductance of two conductors at an angle θ is given by (C.2). The four distances between the ends of the conductors, as shown in Fig.2, are given by (C.3)-(C.6).

3) Mutual inductance between two skewed and displaced conductors [17], [18]: Fig. 3 shows two conductors having similar features of the preceding case except that the conductors are displaced by a distance d. Similar to the last case, the four distances between the ends of the conductors, as shown in Fig. 3, are given by (C.7). The mutual inductance between the conductors having lengths l and m is given by (C.8). The parameter Ω in (C.8) is given by (C.9).

Fig. 2. Two conductors at an angle [17].

This article has been accepted for publication in a future issue of this journal, but has not been fully edited. Content may change prior to final publication. Citation information: DOI 10.1109/JESTPE.2021.3077203, IEEE Journal of Emerging and Selected Topics in Power Electronics

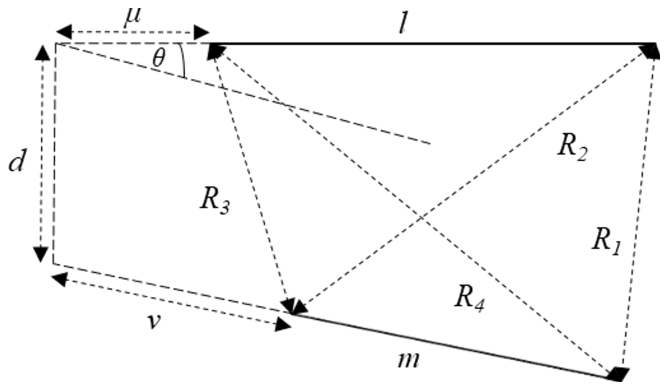

Fig. 3. Two skewed and displaced conductors [17].

The main difference between (C.2) and (C.8) is due to the angle Ω, which vanishes for $d = 0$. In other words, if the displacement between the conductors, d, is zero, then the angle θ between the two conductors is the same as in the previous case.

4) Mutual inductance between two filamentary parallel rectangles [16]: For two equal parallel rectangles of sides a and b, and separation s, the mutual inductance is given by (C.10). For two squares, where $a = b$, (C.10) simplifies to (C.11).

III. ANALYTICAL MODELS

In this section, analytical expressions for the inductances of four different types of inductor structures are developed based on their approximated and actual geometric models (hereinafter together referred to as 'the geometric models'). The geometric models of all four types inductor structures are classified into two categories: (1) *single-turn geometric model (STGM)*: the physical structure employed for computing self-inductance of a single turn and (2) *two-turn geometric model (TTGM)*: the physical structure employed for computing mutual inductance between any two turns. The inductance of each type of inductor structure, as shown in Fig. 1, is the summation of self-inductances of all N-turns and the mutual inductances between all pairs of N-turns.

A. Type 1: Toroidal Inductor with CCSP

This type of inductor was embedded in a silicon substrate with TSVs (referred to as copper pillars in this work) and suspended copper windings (referred to as interconnects in this work) [9].

The geometric models of this inductor structure have the following features: *STGM* considers the actual structure of the turn, as shown in Fig. 4, whereas *TTGM* assumes that the turns are closed, as shown in Fig. 5. We will now walk through the steps involved in determining the self and mutual inductances of this inductor structure by using its geometric models.

1) Self-inductance of a single toroidal turn (L_{1_ST}): L_{1_ST} can be computed by using the *STGM*, as shown in Fig. 4 and is composed of the following components:

(i) *Self-inductance of inner pillar* (L_{ip}) and *outer pillar* (L_{op}): Equation (B.1) can be used to calculate the self-inductance of inner and outer pillars of length, l_p and radius, ρ, given by (1).

$$L_{ip} = L_{op} = L_{circ}(l_p, \rho) \tag{1}$$

(ii) *Self-inductance of the top interconnect (L_{ti}) and the bottom interconnect (L_{bi})*: Similarly, (B.2) can be used to calculate the self-inductance of the top and bottom interconnects having length l_p and rectangular cross sectional dimensions of α_i (width) and β_i (height), given by (2).

$$L_{ti/bi} = L_{rect}(l_{ti/bi}, \alpha_i, \beta_i) \tag{2}$$

(iii) *Mutual inductance between inner and outer pillars* (M_{io_ST}): Mutual inductance between inner and outer pillars can be determined by placing $l = l_p$ and $D = R_o$ - R_i + 2ρ in (C.1) and the resulting expression is:

$$M_{io\_ST} = M_{par}(l_p, R_o - R_i + 2\rho) \tag{3}$$

Where R_i and R_o are the inner and outer radii of the toroidal inductor, respectively. In M_{io_ST}, subscript denotes the case of a single turn (ST).

(iv) *Mutual inductance between the bottom and top interconnects* (M_{bt_ST}): The expressions for the lengths of the top interconnect, l_{ti}, and the bottom interconnect, l_{bi}, are given by (4) and (5), respectively.

$$l_{ti} = R_o - R_i + 2\rho \tag{4}$$

$$l_{bi} = \sqrt{(R_o + \rho)^2 + (R_i - \rho)^2 - 2\,(R_o + \rho)\,(R_i - \rho)\,cos\theta} \tag{5}$$

From Figs. 1(a) and 4, we can see that θ = *360/N*, where *N* is the number of turns.

Therefore, we can calculate the distances between the ends of the bottom and top interconnects, that is, R_{1_ST}, R_{2_ST}, R_{3_ST}, and R_{4_ST}, as illustrated in Fig. 4. Equation (C.7) from the literature can be employed to obtain the expressions for all four distances. By plugging the values $l = l_{ti}$, $m = l_{bi}$, $d = l_p + \beta_i$, μ = *0*, ν = *0*, $\theta_1 \approx \theta = 360/N$ in (C.7), (C.8), and (C.9), we obtain the values of R_{1_ST}, R_{2_ST}, R_{3_ST}, R_{4_ST}, M_{bt_ST}, and Ω_{bt_ST}, respectively and the expressions are given as follows:

$$R_{1\_ST} = \sqrt{(l_p + \beta_i)^2 + r_1(l_{ti}, l_{bi}, 0, 0, 360/N)} \tag{6}$$

$$R_{2\_ST} = \sqrt{(l_p + \beta_i)^2 + r_2(l_{ti}, 0, 0, 360/N)} \tag{7}$$

$$R_{3\_ST} = \sqrt{(l_p + \beta_i)^2 + r_3(0, 0, 360/N)} \tag{8}$$

$$R_{4\_ST} = \sqrt{(l_p + \beta_i)^2 + r_4(l_{bi}, 0, 0, 360/N)} \tag{9}$$

$$M_{bt\_ST} = M_{lm\_2}(l_{ti}, l_{bi}, l_p + \beta_i, 0, 0, 360/N) \tag{10}$$

$$\Omega_{bt\_ST} = \Omega(l_{ti}, l_{bi}, l_p + \beta_i, 0, 0, 360/N) \tag{11}$$

This article has been accepted for publication in a future issue of this journal, but has not been fully edited. Content may change prior to final publication. Citation information: DOI 10.1109/JESTPE.2021.3077203, IEEE Journal of Emerging and Selected Topics in Power Electronics

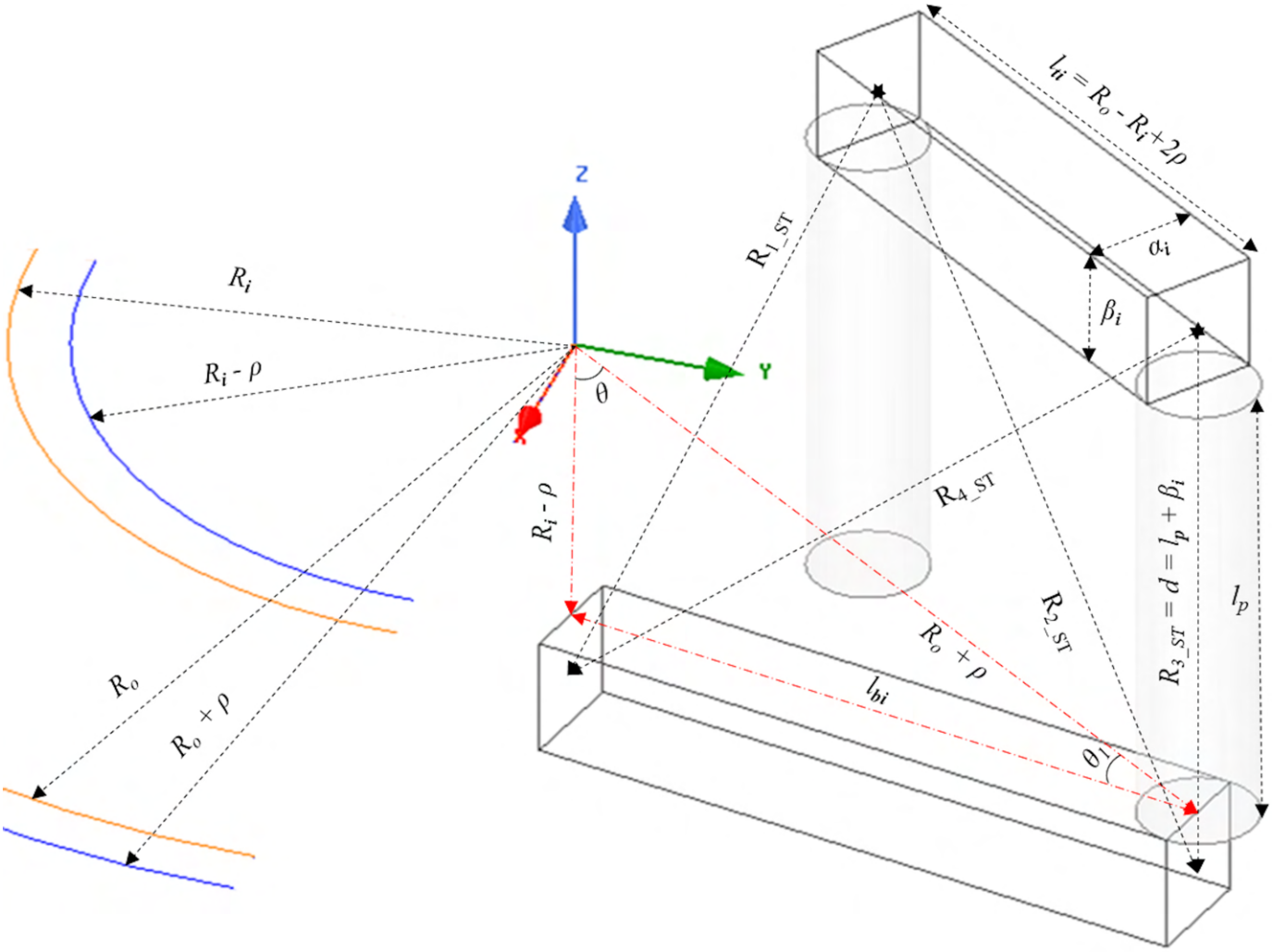

Fig. 4. *Single-turn geometric model (STGM)* of *type 1* for computing the self-inductance of a single-turn.

where d is the center to center distance between the top and bottom interconnects of a single turn and, $d = l_p + \beta_i$, this relation can be easily understood with the help of Fig. 4. The parameter θ_1 is the angle between top and bottom interconnects as shown in Fig. 4. For the sake of brevity, M_{bt_ST} is presented as a function of variables rather than the whole expression; the same holds true for most of the equations presented in this paper.

Finally, L_{1_ST} is the sum of all the components, i.e., $L_{ip} + L_{op} + L_{ti} + L_{bi} - 2M_{io\_ST} - 2M_{bt\_ST}$. The expression for L_{1_ST} is given by

$$\begin{aligned} L_{1\_ST} \;=\; & 2L_{circ}(l_p, \rho) + L_{rect}(l_{ti}, \alpha_i, \beta_i) \\ & + L_{rect}(l_{bi}, \alpha_i, \beta_i) - 2M_{par}(l_p, R_o - R_i + 2\rho) \\ & - 2M_{lm\_2}(l_{ti}, l_{bi}, l_p + \beta_i, 0, 0, 360/N) \end{aligned} \quad (12)$$

All other conductor pair combinations yield zero mutual inductance due to orthogonal currents. Equation (12) can be easily understood with the help of Fig. 9, which is the *STGM* for *type 4* inductor. The *STGM*s of *type 1* and *type 4* are the same. The negative sign in (12) signifies that currents flowing in pillars and interconnects are in opposite directions as illustrated in Fig. 9.

2) Mutual inductance between any two turns at an angle (M_θ): M_θ can be determined by employing the *TTGM*, as shown in Fig. 5. In the *TTGM*, the position of the bottom interconnect is reoriented as an approximation; however, the actual length is preserved. This modification would enable us to employ existing basic equations to find M_θ. The modification provides reasonable accuracy, which is discussed in validation section. While computing M_θ, we can use (5) to determine the bottom interconnect length, l_{bi}. Before proceeding to the determination of M_θ, we should familiarize with mutual inductances of conductors at an angle, and skewed and displaced conductors, which are discussed in section II. M_θ consists of the following components:

(i) *Mutual inductance between bottom interconnects (M_{bi})*: First, we have to calculate the following parameters r_{1b}, r_{2b}, r_{3b} and r_{4b}, which are the distances between the ends of the bottom interconnects as illustrated in Fig. 5. The parameter r_{4b} is not shown on the figure as it is equal to r_{2b}. The expressions for the parameters can be computed by using (C.3)-(C.6). Substitute $l = m = l_{bi}$, $\mu = \nu = R_o + \rho$

This article has been accepted for publication in a future issue of this journal, but has not been fully edited. Content may change prior to final publication. Citation information: DOI 10.1109/JESTPE.2021.3077203, IEEE Journal of Emerging and Selected Topics in Power Electronics

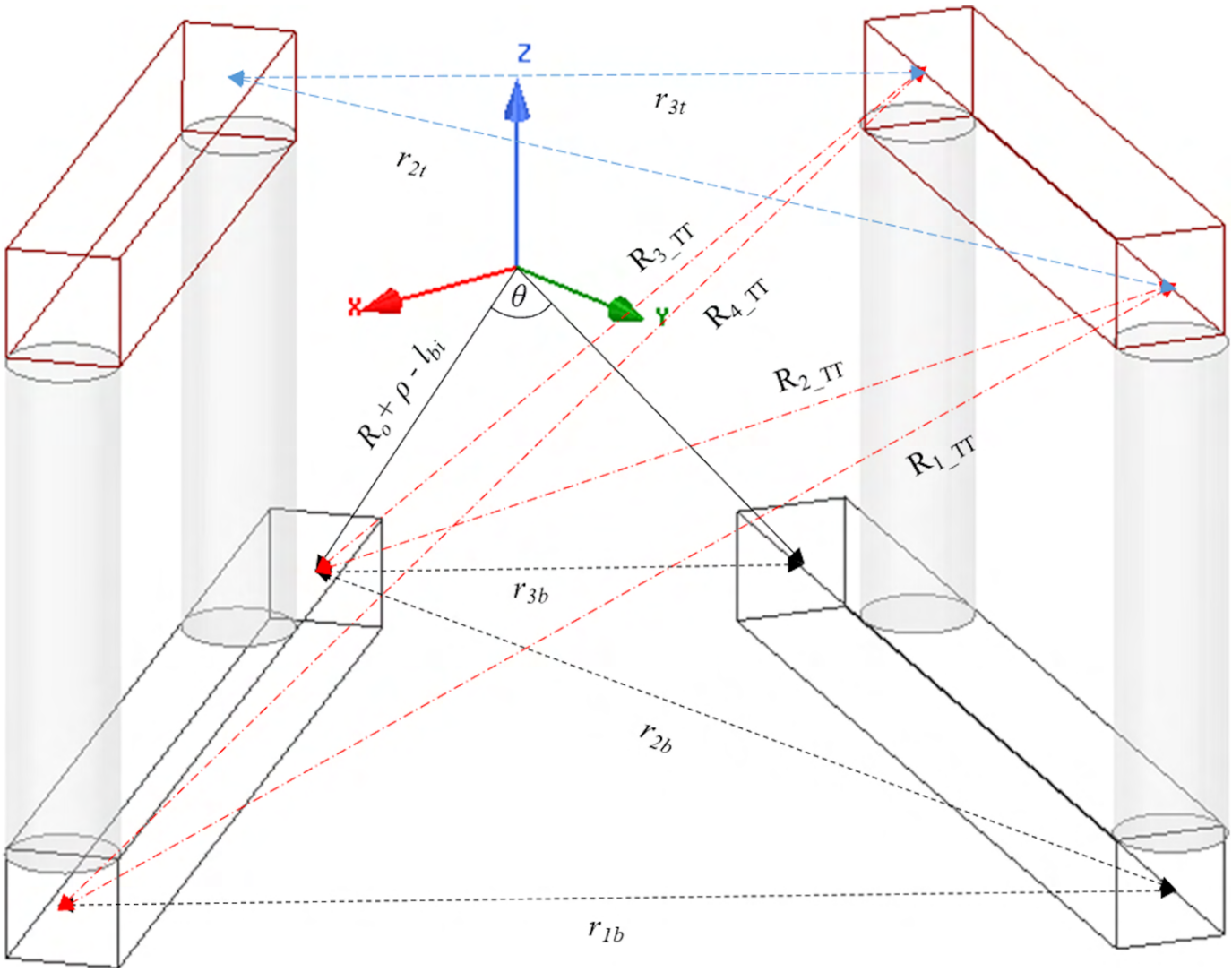

Fig. 5. *Two-turn geometric model (TTGM)* of *type 1* for computing the mutual inductance between any two turns (only the parameters required for the calculation are presented).

- l_{bi}, θ = $360/N$ in (C.2), (C.3), (C.4), (C.5), and (C.6) to get the values of M_{bi}, r_{1b}, r_{2b}, r_{3b} and r_{4b}, respectively. The expressions are given as follows:

$$M_{bi} = M_{lm\_1}(l_{bi}, l_{bi}, R_o + \rho - l_{bi}, R_o + \rho - l_{bi}, 360/N) \tag{13}$$

$$r_{1b} = r_1(l_{bi}, l_{bi}, R_o + \rho - l_{bi}, R_o + \rho - l_{bi}, 360/N) \tag{14}$$

$$r_{2b} = r_{4b} = r_2(l_{bi}, R_o + \rho - l_{bi}, R_o + \rho - l_{bi}, 360/N) \tag{15}$$

$$r_{3b} = r_3(R_o + \rho - l_{bi}, R_o + \rho - l_{bi}, 360/N) \tag{16}$$

(ii) *Mutual inductance between top interconnects (M_{ti})*: Similar to the previous case, first we need to find the distance between the ends of the top interconnects. The distances are denoted by r_{1t}, r_{2t}, r_{3t}, and r_{4t}. The value of r_1 is the same for both top and bottom interconnects, that is, $r_{1t} = r_{1b}$; this is evident from Fig. 5. Also, we should note that $r_{2t} = r_{4t}$. The values of M_{ti}, r_{1t}, r_{2t}, r_{3t} and r_{4t} can be computed by substituting l = m = l_{ti}, μ = ν = R_i - ρ, θ = $360/N$ in (C.2), (C.3), (C.4), (C.5), and (C.6), respectively. The expressions are given by

$$M_{ti} = M_{lm\_1}(l_{ti}, l_{ti}, R_i - \rho, R_i - \rho, 360/N) \tag{17}$$

$$r_{1t} = r_1(l_{ti}, l_{ti}, R_i - \rho, R_i - \rho, 360/N) \tag{18}$$

$$r_{2t} = r_{4t} = r_2(l_{ti}, R_i - \rho, R_i - \rho, 360/N) \tag{19}$$

$$r_{3t} = r_3(R_i - \rho, R_i - \rho, 360/N) \tag{20}$$

(iii) *Mutual inductance between outer copper pillars (M_{op})*: The distance between outer pillars is r_{1b} (given by (14)), which is the same as one of the distances between the ends of the bottom interconnects, as illustrated in Fig. 5. Then we should replace D by r_{1b} in (C.1) to calculate M_{op} and is given by (21).

$$M_{op} = M_{par}(l_p, r_{1b}) \tag{21}$$

We can also use r_{1t} in place of r_{1b} in the above expression since $r_{1t} = r_{1b}$.

This article has been accepted for publication in a future issue of this journal, but has not been fully edited. Content may change prior to final publication. Citation information: DOI 10.1109/JESTPE.2021.3077203, IEEE Journal of Emerging and Selected Topics in Power Electronics

(iv) *Mutual inductance between inner and outer pillars* (M_{io_TT}): In this case, the distance between inner and outer pillars is the same as one of the distances between the ends of the top interconnects, i.e., r_{2t} (given by (19)), as shown in Fig. 5. Next, we should follow the same step as we did in the previous type to find M_{io_TT}. We can also use r_{4t} in place of r_{2t} as $r_{4t} = r_{2t}$. The value of M_{io_TT} is equal to:

$$M_{io\_TT} = M_{par}(l_p, r_{2t}) \tag{22}$$

In M_{io_TT}, subscript denotes the case of a two-turn (TT).

(v) *Mutual inductance between inner pillars* (M_{ip}): The same procedure, described for the above two types, can be used to find M_{ip}. Note that the distance r_{3t} (given by (20)), one of the distances between the ends of top interconnects as illustrated in Fig. 5, is the distance between inner pillars. The value of M_{ip} is equal to:

$$M_{ip} = M_{par}(l_p, r_{3t}) \tag{23}$$

(vi) *Mutual inductance between the bottom and top interconnects* (M_{bt_TT}): We can repeat the same steps that we adapted for finding M_{ti} or M_{bi}. That is, here also we should find the distance between the ends of the top and bottom interconnects. The distances R_{1_TT}, R_{2_TT}, R_{3_TT}, and R_{4_TT} of the bottom and top interconnects, as illustrated in Fig. 5, can be calculated from (C.7). Substitute l = l_{ti}, m = l_{bi}, μ = R_i - ρ, ν = R_o + ρ - l_{bi}, $d = l_p + \beta_i$, $\theta = 360/N$ in (C.7), (C.8), and (C.9) to get the expression for R_{1_TT}, R_{2_TT}, R_{3_TT}, R_{4_TT}, M_{bt_TT}, and Ω_{bt_TT}, respectively. The expressions are given by

$$R_{1\_TT} = \sqrt{d^2 + r_1(l_{ti}, l_{bi}, R_i - \rho, R_o + \rho - l_{bi}, \theta)} \tag{24}$$

$$R_{2\_TT} = \sqrt{d^2 + r_2(l_{ti}, R_i - \rho, R_o + \rho - l_{bi}, \theta)} \tag{25}$$

$$R_{3\_TT} = \sqrt{d^2 + r_3(R_i - \rho, R_o + \rho - l_{bi}, \theta)} \tag{26}$$

$$R_{4\_TT} = \sqrt{d^2 + r_4(l_{bi}, R_i - \rho, R_o + \rho - l_{bi}, \theta)} \tag{27}$$

$$M_{bt\_TT} = M_{lm\_2}(l_{ti}, l_{bi}, d, R_i - \rho, R_o + \rho - l_{bi}, \theta) \tag{28}$$

$$\Omega_{bt\_TT} = \Omega(l_{ti}, l_{bi}, d, R_i - \rho, R_o + \rho - l_{bi}, \theta) \tag{29}$$

Finally, M_θ is the sum of all the above components and is equal to:

$$\begin{aligned} M_\theta \quad = \quad & 2M_{bi} + 2M_{ti} + 2M_{op} - 4M_{io\_TT} \\ & + 2M_{ip} - 4M_{bt\_TT} \end{aligned} \tag{30}$$

Equation (30) can be easily understood with the help of Fig. 7, which is the *TTGM* for *type 2* inductor, as the components of M_θ are the same for *type 1* and *type 2* inductors. The mutual inductance contribution from all the pairs of turns can be expressed as:

$$M_{1\_e} = N\left(M_\theta + M_{2\theta} \cdots M_{\left(\frac{N}{2}-1\right)\theta}\right) + \left(\frac{N}{2}\right) M_{180} \tag{31}$$

$$M_{1\_o} = N\left(M_\theta + M_{2\theta} + M_{3\theta} \cdots\cdots\cdots\cdots M_{\left(\frac{N-1}{2}\right)\theta}\right) \tag{32}$$

in which M_θ is the mutual inductance between the turns having angle θ, $M_{2\theta}$ is the mutual inductance between the turns having angle 2θ and so on.

Equations (31) and (32) are expressions for the net mutual inductance for an inductor having an even number of turns, and an odd number of turns, respectively. The total inductance of the whole inductor structure is given by (33) for an even number of turns and (34) for an odd number of turns.

$$L_{1\_e} = NL_{1\_ST} + M_{1\_e} \tag{33}$$

$$L_{1\_o} = NL_{1\_ST} + M_{1\_o} \tag{34}$$

B. Type 2: Toroidal Inductor with RCSP

Silicon-embedded 3D inductors can be fabricated using a lithography-based process or a shadow-mask-based process; the shadow mask approach reduces process time [11], [25]. Since the shadow mask based process does not support circular features [26], rectangular cross section geometries can be chosen while employing this approach in order to reduce overall processing time.

For the *type 2* inductor structure, new geometric models are adapted for computing self and mutual inductances. The *STGM* and *TTGM* of *type 2* are shown in Figs. 6 and 7, respectively. There are two subtle differences between the *type 2* and *type1* inductors' *STGM* and *TTGM*: 1) in the *STGM* of *type 2*, the turn is completely closed, whereas in the case of *type 1* the actual structure of the turn, without any physical approximation, is considered and (2) when it comes to *TTGM*, for both types the turns are completely closed; however, in *type 2* the bottom interconnect length is approximated as equal to the top interconnect length, i.e., $l_{bi} = l_{ti} = R_o - R_i + \beta_p$, while in the case of *type 1*, the actual length of the bottom interconnect is considered, i.e., $l_{bi} = \sqrt{(R_o+\rho)^2 + (R_i-\rho)^2 - 2(R_o+\rho)(R_i-\rho)cos\theta}$. In fact, the actual length of the bottom interconnect is larger than the top interconnect length in both types of inductors.

The *TTGM*s of *type 2* and *type 1* are interchangeable. The *TTGM* of *type 2* was employed to find the net mutual inductance of *type 1*. The FEA solution demonstrates that the mutual inductance predicted by *TTGM* of *type 2* is 5% less accurate compared to that of *TTGM* of *type 1*. For the comparison, we used the specifications of an example inductor with even turns, which are given in Table I of section IV. On the other hand, the advantage of the *TTGM* of *type 2* is the reduced complexity, which is discussed later in this section while comparing *TTGM*s *type 1* and *type 2*.

The *STGM*s are specific to the inductor types. In other words, the *STGM*, shown in Fig. 6, is more suitable for *type 2* structure. Because in this configuration the structure is uniform, that is, pillars and interconnects have the same geometry; in this case, it's rectangular geometry.

Now, we derive the expressions for the self-inductance of a single turn and the mutual inductance between any two turns.

1) Self-inductance of single turn (L_{2_ST}): In section II, the inductance formulae for rectangular loops of various types are discussed. Equation (B.3) is used to find L_{2_ST}. Substitute

This article has been accepted for publication in a future issue of this journal, but has not been fully edited. Content may change prior to final publication. Citation information: DOI 10.1109/JESTPE.2021.3077203, IEEE Journal of Emerging and Selected Topics in Power Electronics

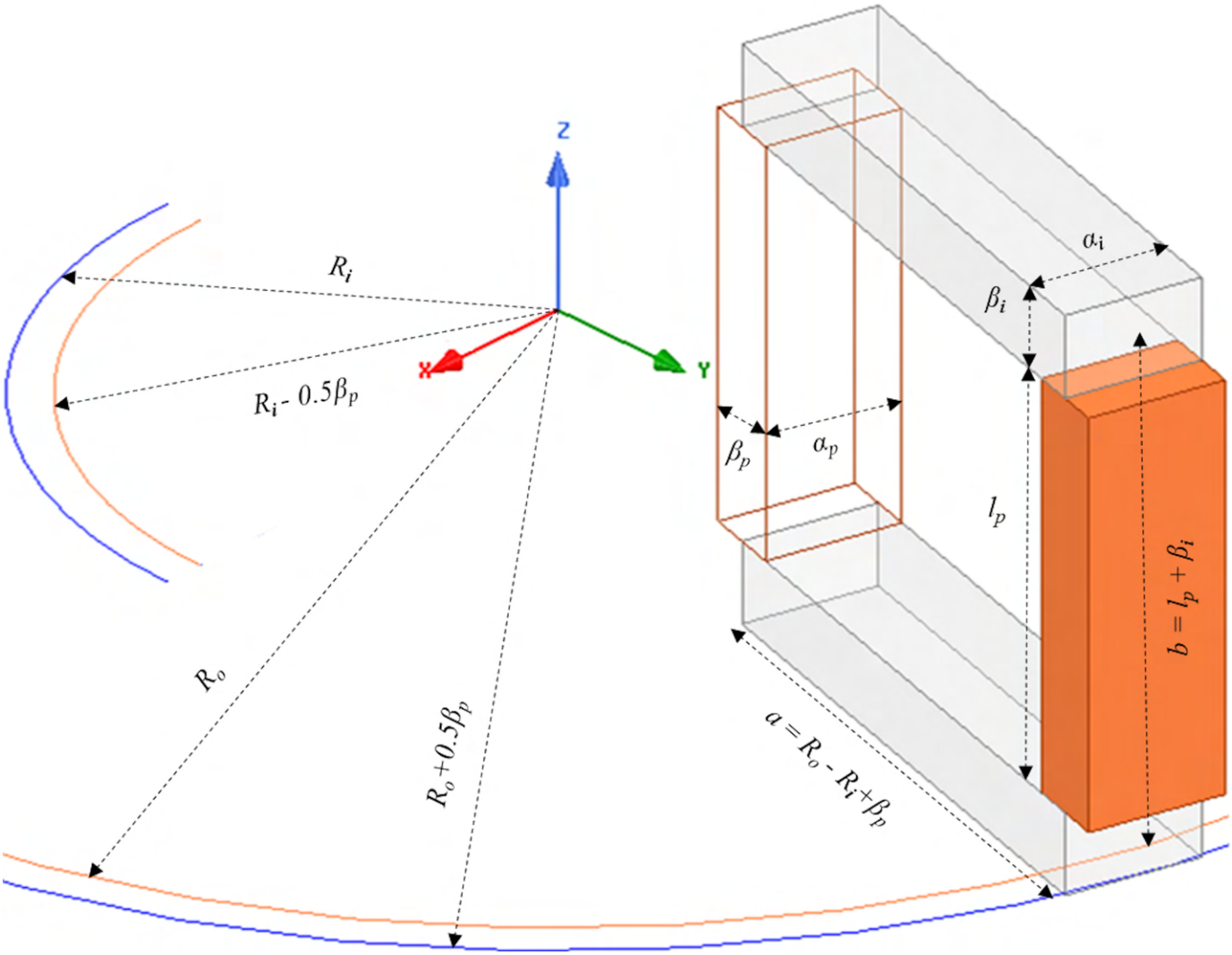

Fig. 6. *Single-turn geometric model (STGM)* of *type 2* for computing the self-inductance of a single-turn.

$a = R_o - R_i + \beta_p$, $b = l_p + \beta_i$, $\alpha_a = \alpha_i$, $\beta_a = \beta_i$, $\alpha_b = \alpha_p$, and $\beta_b = \beta_p$ in (B.3), where l_p, α_i, β_i, α_p, and β_p are the length of the copper pillar, the width of the interconnect, the height of the interconnect, the width of the copper pillar, and the height of the copper pillar, respectively. This results in an expression for the self-inductance of a single turn, which is a rectangular shape and composed of rectangular cross section conductors. The expression is equal to:

$$L_{2\_ST} = L_{RECT\_1}(R_o - R_i + \beta_p, l_p + \beta_i, \alpha_i, \beta_i, \alpha_p, \beta_p) \quad (35)$$

2) Mutual inductance between any two turns: The same procedure used to find the mutual inductance between any two turns of the *type 1* inductor can be adapted here. However, there is a fine distinction between the *TTGM*s of *type 2* and the *type 1* inductors, which has been explained in detail while introducing this inductor. The differences can be noticed by comparing Figs. 5 and 7. As far as the computation of mutual inductance is concerned, the differences and similarities between the parameters of the *TTGM*s of *type 1* and *type 2* can be summarized as follows:

- The distances r_1, r_2, r_3 and r_4 for both bottom and top interconnects are the same for *TTGM* of *type 2*; that is, $r_{1b} = r_{1t}$, $r_{2b} = r_{2t}$, $r_{3b} = r_{3t}$, and $r_{4b} = r_{4t}$. However, in *TTGM* of *type1*, only r_1 is the same for both bottom and top interconnects, i.e., $r_{1b} = r_{1t}$.
- The values of r_2 and r_4 are equal for both top and bottom interconnects of *type 2* as well as *type 1*: that is, $r_{2t} = r_{4t}$ and $r_{2b} = r_{4b}$ for both models.
- In *type 2*, the distance between inner pillars is r_3 of top interconnects or bottom interconnects (i.e., r_{3t} or r_{3b}), whereas in *type 1*, it is r_3 of top interconnects (i.e., r_{3t}). The distance between outer pillars is the same as r_1 of top interconnects or bottom interconnects for both types.
- For *type 1*, the values of R_{1_TT}, R_{2_TT}, R_{3_TT}, and R_{4_TT}, which are the distance between the ends of the bottom and top interconnects as shown in Fig. 5, are distinct. In the case of *type 2*, R_{2_TT} = R_{4_TT}.
- The term ρ must be replaced by $0.5\beta_p$, as illustrated in Fig. 7, in all the set of equations, which are employed for finding the mutual inductance between any two turns of *type 1*, in order to apply for *type 2*.

This article has been accepted for publication in a future issue of this journal, but has not been fully edited. Content may change prior to final publication. Citation information: DOI 10.1109/JESTPE.2021.3077203, IEEE Journal of Emerging and Selected Topics in Power Electronics

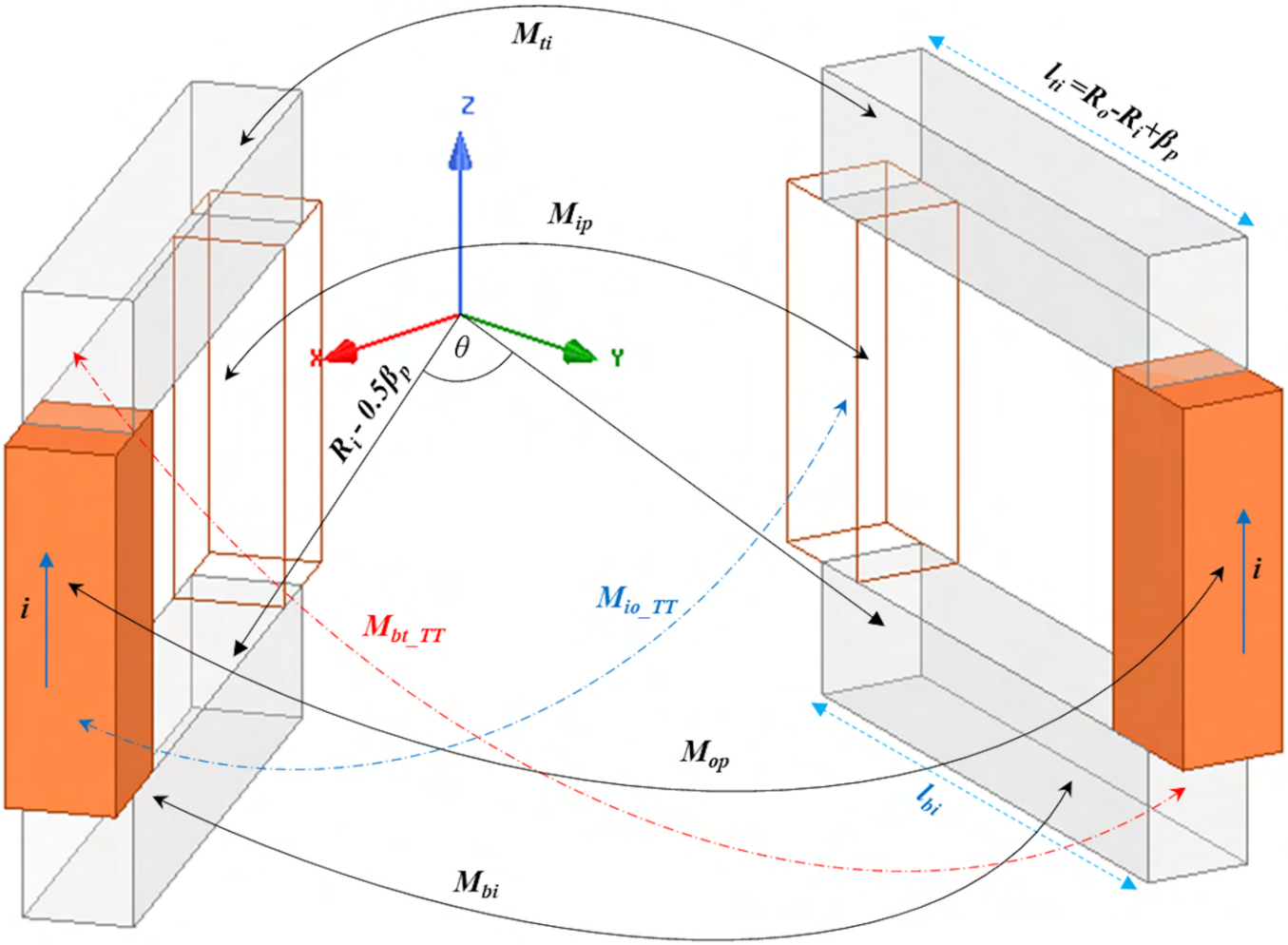

Fig. 7. *Two-turn geometric model (TTGM)* of *type 2* for computing mutual inductance between any two turns.

Finally, the mutual inductances of all the pairs of turns can be calculated from (31) or (32) and total inductance of the inductor structure can be calculated from (33) or (34), depending on the number of turns is even or odd.

C. Type 3: Solenoid Inductor with RCSP

The *Type 3* was embedded in a Si substrate; the copper pillars and interconnects are developed through deep Si etching and Cu electroplating [12].

For this type also we will consider closed turn geometric models for determining both self and mutual inductances as we did for the *type 2*. Here also, the bottom interconnect length is taken as equal to the top interconnect length, similar to the case of *type 2*. The approximated geometric models for this type of inductor are shown in Fig. 8. The analytical models for inductances of square and rectangular solenoid inductor structures are discussed here.

We derive the expressions for the self-inductance of a single turn and the mutual inductance between any two turns.

1) Self-inductance of a single turn (L_{3_ST}): As the *STGM*, Fig. 8(a), of this type of inductor is similar to that of second type of inductor, we can follow the same steps. The main difference between the geometric models of the two types is that the turn of this type has uniform cross section; the copper pillars and interconnects have the same cross section: $(\alpha+\beta)_p = (\alpha+\beta)_i$. Also, the design parameters are different. Substitute $\alpha = \alpha_p = \alpha_i$, $\beta = \beta_p = \beta_i$, $a = p$, and $b = l_p + \beta_i = l_p + \beta_p = l_p + \beta$ in (B.4), where α_p, β_p, α_i, β_i, p, and l_p are width of the pillar, height of the pillar, width of the interconnect, height of the interconnect, pitch of the solenoid turns, and length of the pillar, respectively. This results in the expression for the self-inductance of a single turn of rectangular solenoid inductor structure with rectangular cross section pillars being given by

$$L_{3\_ST(rect)} = L_{RECT\_2}(p, l_p+\beta, \alpha, \beta) \tag{36}$$

Similarly, we can develop the expression for the self-inductance of a single turn of square solenoid inductor structure with square cross sectional pillars by substituting $a = p$ and $\alpha = \alpha_i = \alpha_p = \beta_i = \beta_p$ in (B.6). The resulting expression is equal to:

This article has been accepted for publication in a future issue of this journal, but has not been fully edited. Content may change prior to final publication. Citation information: DOI 10.1109/JESTPE.2021.3077203, IEEE Journal of Emerging and Selected Topics in Power Electronics

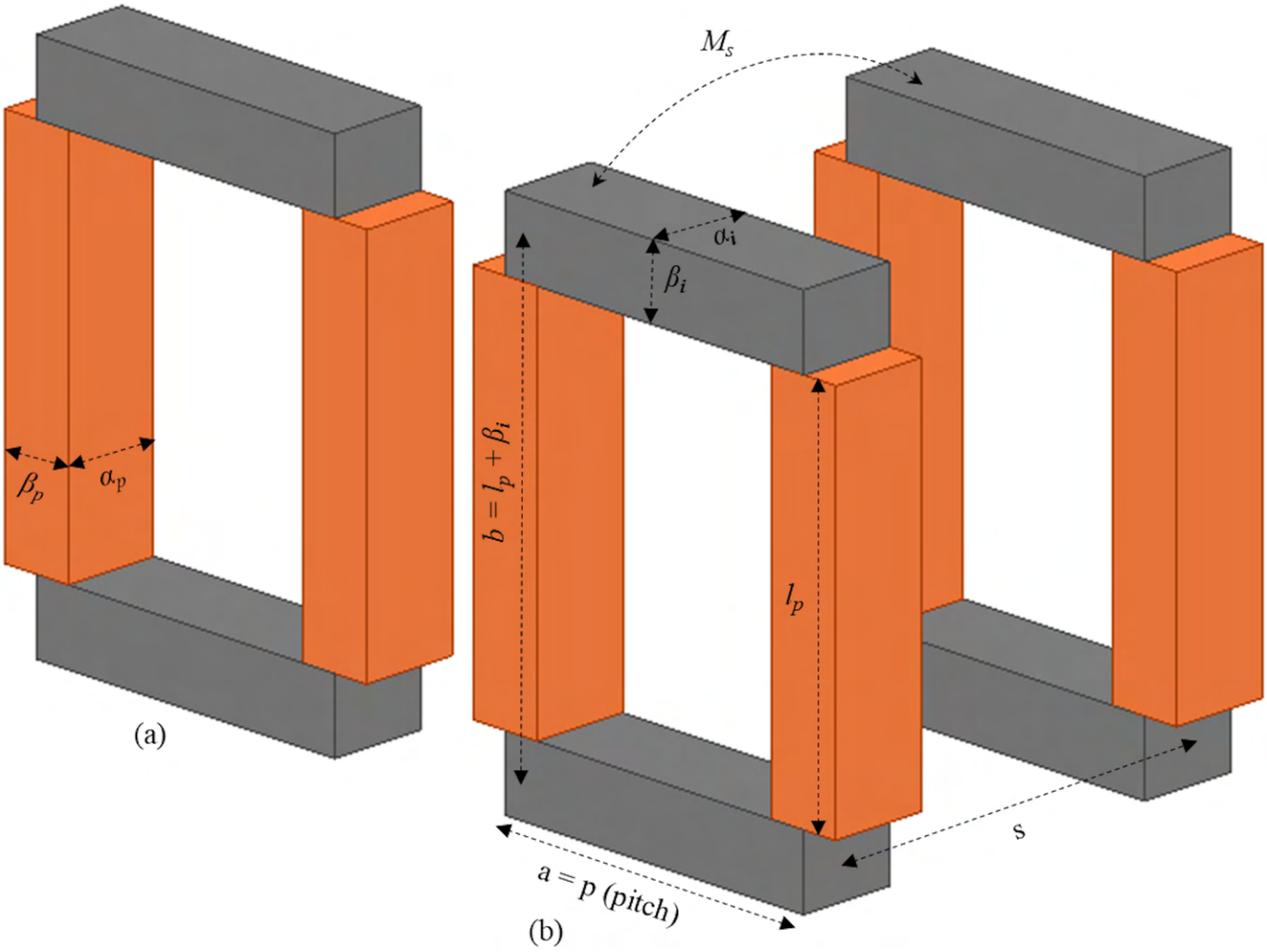

Fig. 8. (a) *Single-turn geometric model (STGM)*. (b) *Two-turn geometric model (TTGM)* of *type 3*.

$$L_{3\_ST(sq)} = L_{sq\_2}(p, \alpha) \tag{37}$$

If the cross section of the conductors (pillars and interconnects) of the turn is non-uniform as in the second type, we can use (B.3) to develop the analytical equation for the inductance of a single turn with proper substitution of design parameters.

2) Mutual inductance between any two turns (M_s): The *TTGM* of *type 3* is shown in Fig. 8(b). This model resembles two parallel square or rectangular loops. This implies that we can apply (C.10) and (C.11) to find the mutual inductance between parallel rectangular turns, and square turns, respectively.

By substituting $a = p$, $b = l_p + \beta_i$ and $s = s$ in (C.10) and (C.11), we get the expressions for mutual inductance between rectangular shape turns, $M_{s(rect)}$, and square shape turns, $M_{s(sq)}$, respectively and can be written as:

$$M_{s(rect)} = M_{rect}(p, l_p + \beta_i, s) \tag{38}$$

$$M_{s(sq)} = M_{sq}(p, s) \tag{39}$$

where s is the turn spacing.

The net mutual inductance of the *type 3* inductor, M_3, is given by

$$M_3 = 2\Big((N-1)M_S + (N-2)M_{2S} + (N-3)M_{3S}\cdots + \cdots + (N-(N-1))M_{(N-1)S}\Big) \tag{40}$$

where M_s is mutual inductance between the turns with spacing s, M_{2s} is mutual inductance between the turns with spacing $2s$ and so on.

The total inductance of the inductor structure can be estimated by

$$L_3 = NL_{3\_ST} + M_3 \tag{41}$$

D. Type 4: Solenoid Inductor with CCSP

For this type of inductor architecture, the top and bottom interconnects are formed using metal tracks and the pillars are produced by TSVs [13]. The geometric models of this type of inductor are shown in Fig. 9. The computation of self and mutual inductances for this type of inductor is described below.

1) Self-inductance of a single turn (L_{4_ST}): The *STGM* for this type of inductor is same as that of first type; however, the design parameters are different as illustrated in Fig. 9(a). For calculating L_{4_ST}, we can follow the similar steps that we did for the first type. The steps are described below:

(i) Equations (B.1) and (B.2) can be used for determining the self-inductance of pillars and interconnects, respectively.
(ii) The same set of equations that we used in the first type inductor can be reconsidered here, that is, (6)-(11) for computing mutual inductance between the top and bottom interconnects. But the parameters, such as top interconnect length (l_{ti}), bottom interconnect length (l_{bi}), and the angle between the top and bottom interconnects (θ), in these equations will have new values: $l_{ti} = p$, $l_{bi} = \sqrt{p^2 + s^2}$, $cos\theta = p/\sqrt{p^2 + s^2}$. The value of d, equal to $l_p + \beta_i$, in (6)-(11) remains unchanged.
(iii) The mutual inductance between the inner and outer pillars can be computed by (C.1).
(iv) Finally, (12) can be used to calculate L_{4_ST}.

2) Mutual inductance of any two turns (M_s): The *TTGM* of this type of inductor, as shown in Fig. 9(b), is similar to that of third type. The only difference between the *TTGM*s of this inductor and *type 3* is that pillars and interconnects of the former are of different cross sections: pillars are circular and interconnects are rectangular, whereas pillars and interconnects of the later are of rectangular cross section. Since the mutual inductance is independent of the cross section of the conductors (a simplifying assumption), we can use the same equations that were employed in *type 3* to determine the mutual inductance of any two turns; that is, we can employ either (38) or (39), depending on the type of turns (i.e., rectangular or square shape).

The net mutual inductance and in turn the total inductance of the whole structure can be determined by (40) and (41), respectively.

IV. MODEL VALIDATION

The proposed analytical models for the inductances of all four types of inductor structures are validated here. Our measurement values, previously published measurement data, and FEA solutions from this work are considered for the model validation. The performance of our models is compared with the conventional analytical expressions, commonly used for calculating large size toroidal and solenoid inductors, to demonstrate the significance of proposed models in calculating the inductance of 3D micro fabricated inductors. Also, the accuracy of the analytical model of *type 4* is compared with previously published models.

The simulations are performed at low frequencies. The measured inductance values from the references at lower frequencies of the given frequency range are considered for the comparison. Effects of high frequency on inductance are discussed in section VI.

A. Type 1

The results of the inductance obtained from analytical model and field solver simulation of this work are compared with those provided by experimental test described in [10]. Also, the accuracy of the proposed analytical model is compared with conventional expression for the inductance of a toroidal inductor, given by (A.1). The same set of specifications of the example inductors from [10] are considered, as given in Table I, in order to make the comparison. In [10], the top and bottom interconnects of the fabricated inductors are trapezoidal slabs. However, in our model we considered rectangular cross section top and bottom interconnects. We had to adapt this modification as there is no precise analytical expression for the inductance of trapezoidal slabs. Also, the characterization of an inductor with trapezoidal cross section interconnects in ANSYS Maxwell requires relatively higher simulation time and memory. The changeover from trapezoidal to rectangular interconnect in our model contributes to the error when compared to the measurement result which is apparent from comparison tables of design examples. Tables II and III show comparison results for the example inductors with even turns and odd turns, respectively. Fig. 10 shows the mutual inductances of the pillars and interconnects of the example inductor with even turns.

TABLE I
DIMENSIONS OF THE EXAMPLE INDUCTORS FOR *TYPE 1*

Design Parameter	**Value**	
	Example inductor with even turns [10]	Example inductor with odd turns [10]
Number of turns (N)	20	25
Inner radius of the toroid (R_i)	750	-
Outer radius of the toroid (R_o)	1500	-
Length of the copper pillar (l_p)	280	-
Copper pillar radius (ρ)	15	-
Top interconnect dimensions ($l_{ti} \times \alpha_i \times \beta_i$)	780 × 30 × 30	-
Bottom interconnect dimensions ($l_{bi} \times \alpha_i \times \beta_i$)	847 × 30× 30	824 × 30× 30

All dimensions are in micrometers (μm).

TABLE II
COMPARISON OF INDUCTANCE FROM OUR MODEL, CONVENTIONAL MODEL, SIMULATION, AND MEASUREMENT OF EXAMPLE INDUCTOR WITH EVEN TURNS FOR *TYPE 1*

	Simulation (32.03 nH)	Measurement@1 MHz [10] (36.24 nH)
Our Model (30.41 nH)	5.06%	16.09%
Conventional Model (A.1)[1] (17.19 nH)	46.33%	52.56%

[1] Refer to the Appendix A. Only the first term of (A.1) is considered for the calculation as we are interested in low frequency inductance value for the comparison.

B. Type 2

The proposed analytical model inductance value is correlated with the simulation of this work and the measured value from [25]. The accuracy of the proposed analytical model is also compared with (A.1). Table IV shows the design parameters of the example inductor from [25]. The comparison

This article has been accepted for publication in a future issue of this journal, but has not been fully edited. Content may change prior to final publication. Citation information: DOI 10.1109/JESTPE.2021.3077203, IEEE Journal of Emerging and Selected Topics in Power Electronics

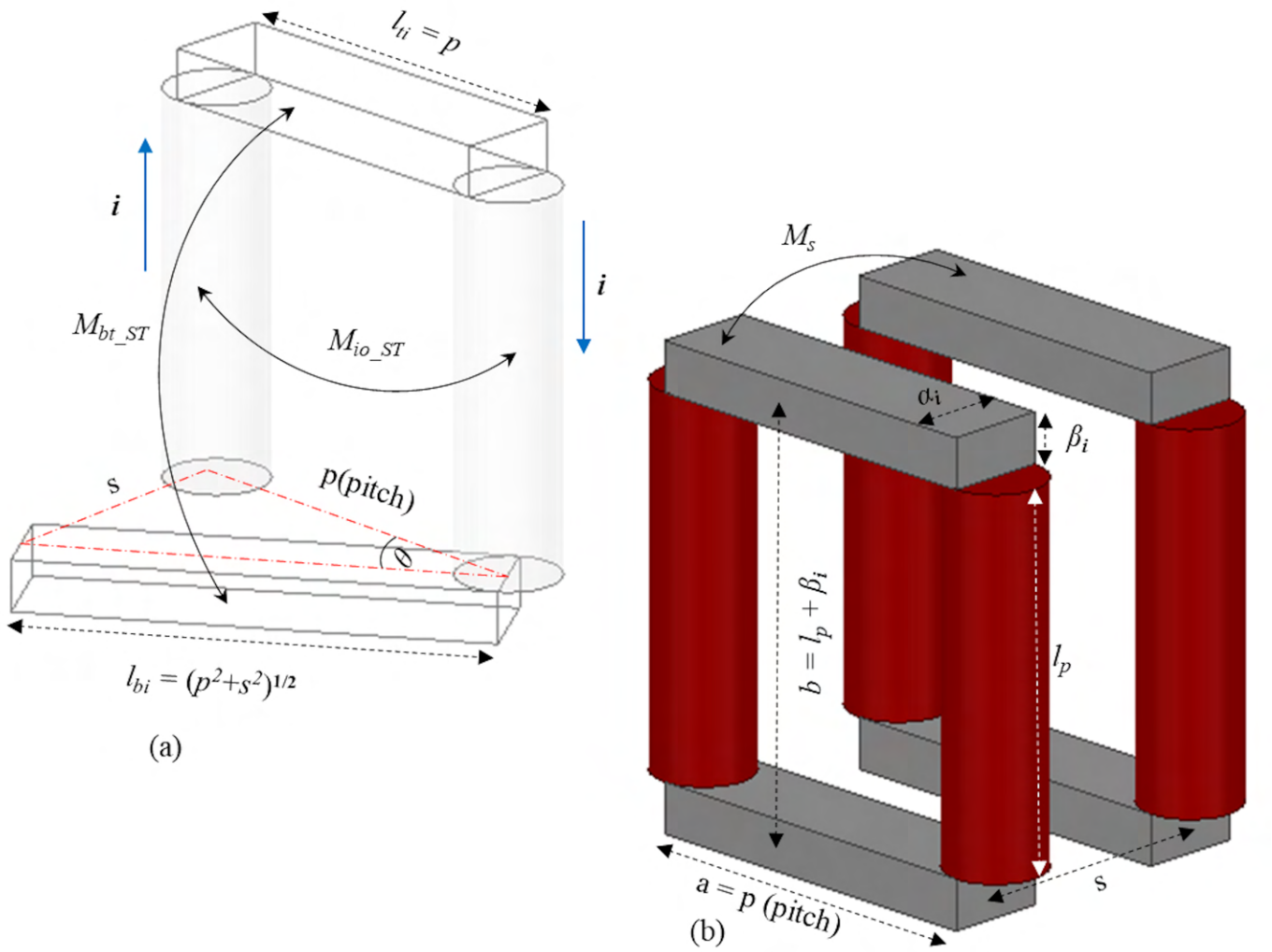

Fig. 9. (a) *Single-turn geometric model (STGM)*. (b) *Two-turn geometric model (TTGM)* of *type 4*.

TABLE III
COMPARISON OF INDUCTANCE FROM OUR MODEL, CONVENTIONAL MODEL, SIMULATION, AND MEASUREMENT OF EXAMPLE INDUCTOR WITH ODD TURNS FOR *TYPE 1*

	Simulation (43.17 nH)	Measurement@1 MHz [10] (41.69 nH)
Our Model (40.67 nH)	5.79%	2.44%
Conventional Model (A.1) (26.85 nH)	37.80%	35.59%

TABLE V
COMPARISON OF INDUCTANCE FROM OUR MODEL, CONVENTIONAL MODEL, SIMULATION, AND MEASUREMENT OF EXAMPLE INDUCTOR FOR *TYPE 2*

	Simulation (63.42 nH)	Measurement@1 MHz [25] (60 nH)
Our Model (59.12 nH)	6.78%	1.47%
Conventional Model (A.1) (42.57 nH)	32.87%	29.05%

results are shown in Table V. Fig. 11 shows the mutual inductances of copper pillars and interconnects of the example inductor.

TABLE IV
DIMENSIONS OF THE EXAMPLE INDUCTOR FROM [25] FOR *TYPE 2*

Design Parameter	**Value**
Number of turns (N)	25
Inner radius of the toroid (R_i)	1000
Outer radius of the toroid (R_o)	3000
Copper pillar dimensions ($l_p \times \alpha_p \times \beta_p$)	300 × 160 × 120
Interconnect dimensions ($l_{ti} \times \alpha_i \times \beta_i$)	2120 × 160 × 20

All dimensions are in micrometers (μm).

C. Type 3

The inductance values from the analytical model and the FEA solution of this work are compared with experimental result of [12]. Also, the accuracy of the proposed analytical model is compared with conventional expression for the inductance of solenoid inductor, i.e., (A.2). Table VI shows the comparison result. The dimensions of the inductor to verify the analytical model are taken from [12] and are reproduced here: 1 mm is the height, two different widths ($0.5/1$ mm), cross section of the conductors (pillars and interconnects) is 100 μm × 100 μm, the spacing between turns, s, is 200 μm and four different turns (5/10/15/20). Variation of mutual

This article has been accepted for publication in a future issue of this journal, but has not been fully edited. Content may change prior to final publication. Citation information: DOI 10.1109/JESTPE.2021.3077203, IEEE Journal of Emerging and Selected Topics in Power Electronics

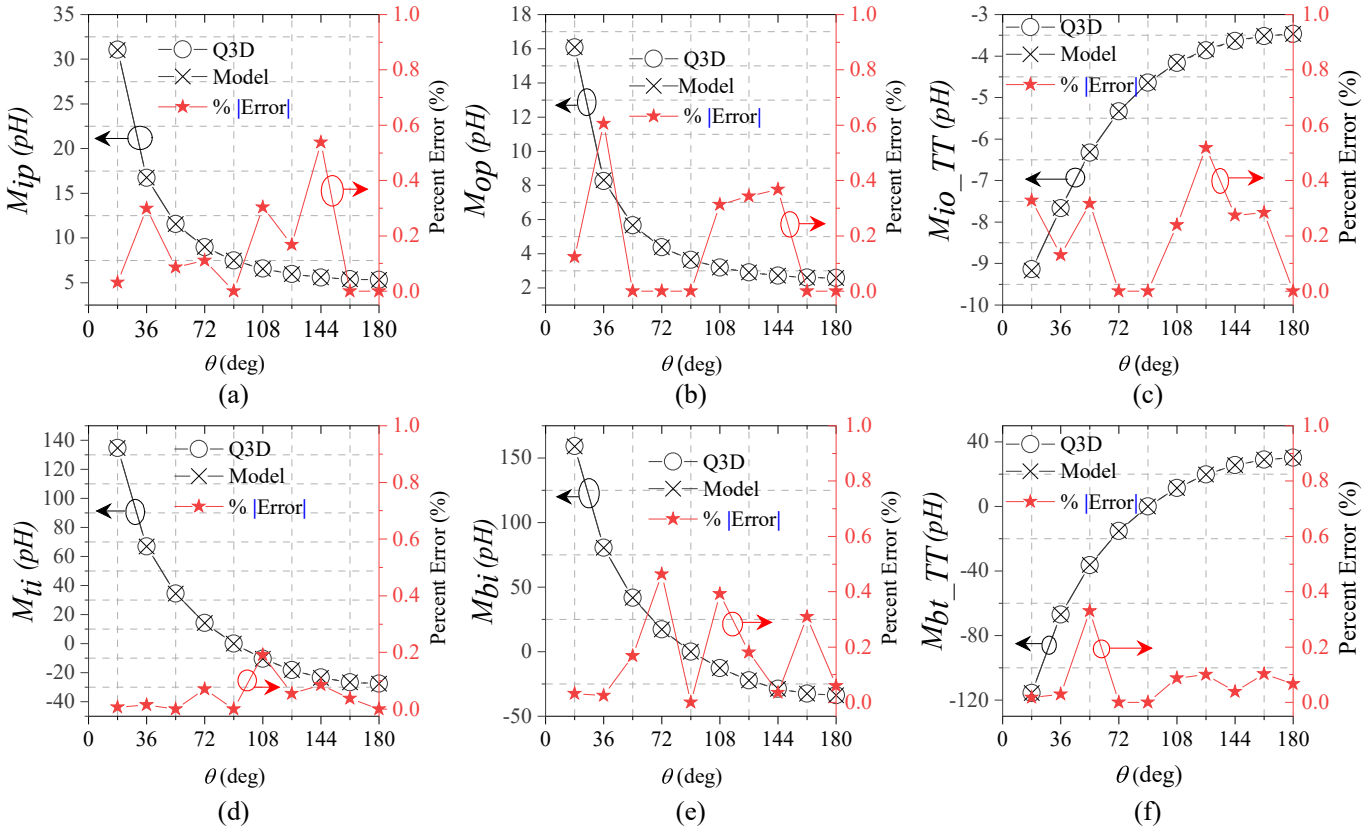

Fig. 10. Plot showing the components of the mutual Inductance between any two turns of the design example (even turns) of *type 1*: Mutual inductance between (a) inner pillars (b) outer pillars (c) inner and outer pillars (d) top interconnects (e) bottom interconnects (f) bottom and top interconnects.

inductance with the spacing between the turns of rectangular solenoid inductor structure (design example with dimension $0.5\ mm \times 1\ mm$) and square solenoid inductor structure (design example with dimension $1\ mm \times 1\ mm$) are shown in Fig. 12(a) and (b), respectively.

The developed analytical model is corresponding to the air core. However, in [12] the inductors are fabricated in a silicon substrate. To put it another way, these are silicon core inductors. Since silicon has high resistivity, the effect of eddy currents on the inductance is not significant over the frequency range of 1-100 MHz. The effects of high frequency on the inductance of air core and silicon core inductors are discussed in section VI.

D. Type 4

The performance of the proposed analytical model is compared with the conventional model, (A.2), as well as the previous models from [14], [15], as shown in Table VII. The design parameters, reproduced from [15], are l_p of 200 μm, ρ of 10 μm, α_i of 20 μm, β_i of 4 μm, p of 300 μm, s of 40 μm. There is a minuscule difference between the physical structures of the inductors from this work, [14], and [15]. Consequenctly, the Q3D results are different. The difference is negligibly small, which is evident from second and third columns of Table VII; nevertheless, this work, [14], and [15] analytical model results are compared with their corresponding Q3D results. Fig. 13 depicts the variation of mutual inductance with the spacing between the turns.

The analytical model from [15] considers an extra term, i.e., internal inductance, in the expression (equation (3)) for the inductance of a rectangular cross section conductor, referred to as "RDL interconnect" in [15]. We have presented the corrected inductance values, by removing the contribution from the added extra term, in Table VII. We have put an effort to demonstrate that the inductance expression (equation (B.2)) for a rectangular conductor, adapted in this work, is more accurate compared to (3) from [15] by comparing inductance values predicted by the expressions and simulation; Table VIII illustrate the comparison results. The results demonstrate that the accuracy of (B.2) from this work is around 7× higher than (3) from [15]. The specifications of the rectangular conductor, reproduced from [15], are as follows: cross section is 20 μm × 4 μm and the length is 300 μm, which is equal to the pitch.

From Table VII, we see that our model is more accurate than the models from [14], [15]. The maximum error is 1.78%. This value is 6× and 2× smaller than the errors introduced by analytical models from [14] and [15], respectively. The reason for the improved in accuracy compared to [15] can be explained as follows. In [15], the computation of mutual inductance between any two turns requires calculation of mutual inductance between 6 pairs of conductors. Consequently,

This article has been accepted for publication in a future issue of this journal, but has not been fully edited. Content may change prior to final publication. Citation information: DOI 10.1109/JESTPE.2021.3077203, IEEE Journal of Emerging and Selected Topics in Power Electronics

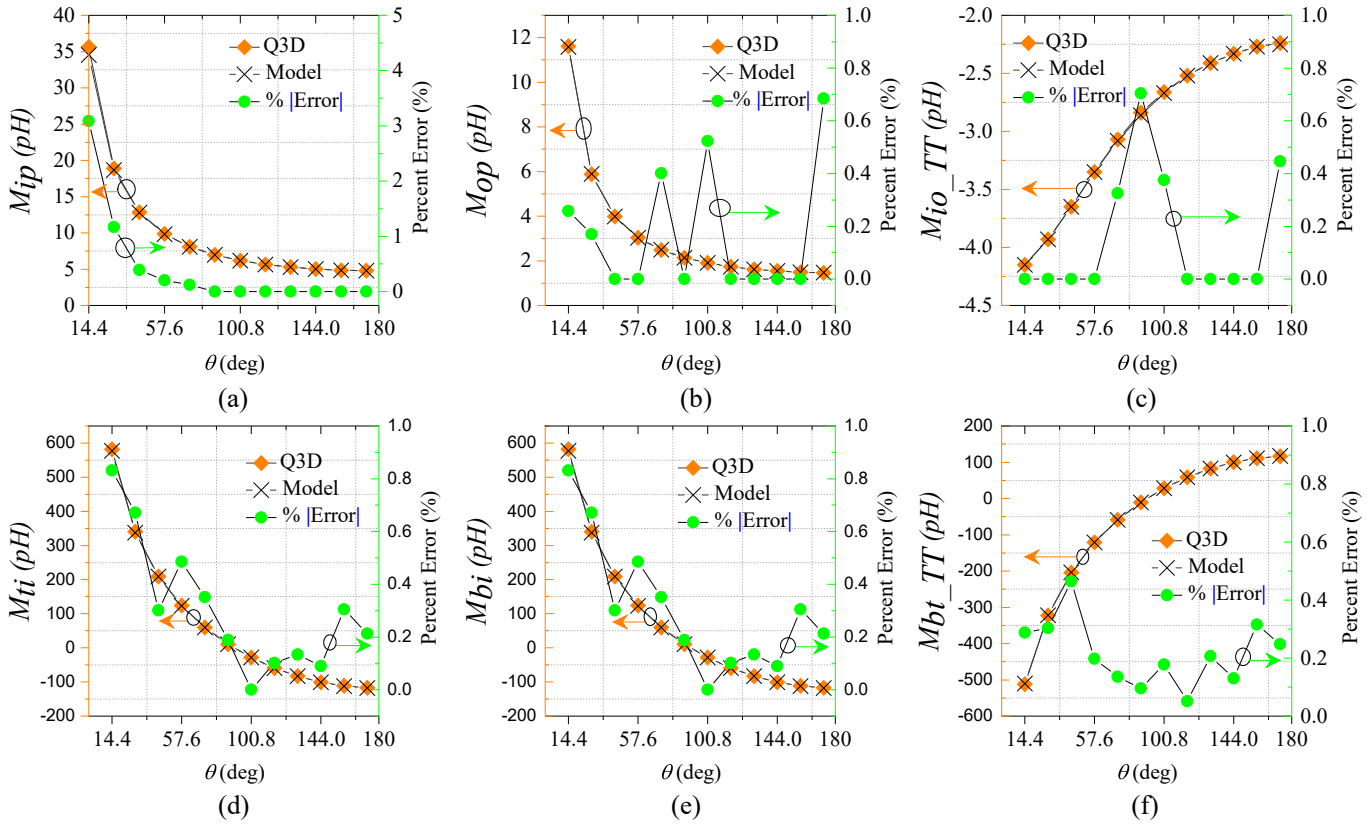

Fig. 11. Plot showing the components of the mutual Inductance between any two turns of the design example of *type 2*: Mutual inductance between (a) inner pillars (b) outer pillars (c) inner and outer pillars (d) top interconnects (e) bottom interconnects (f) bottom and top interconnects.

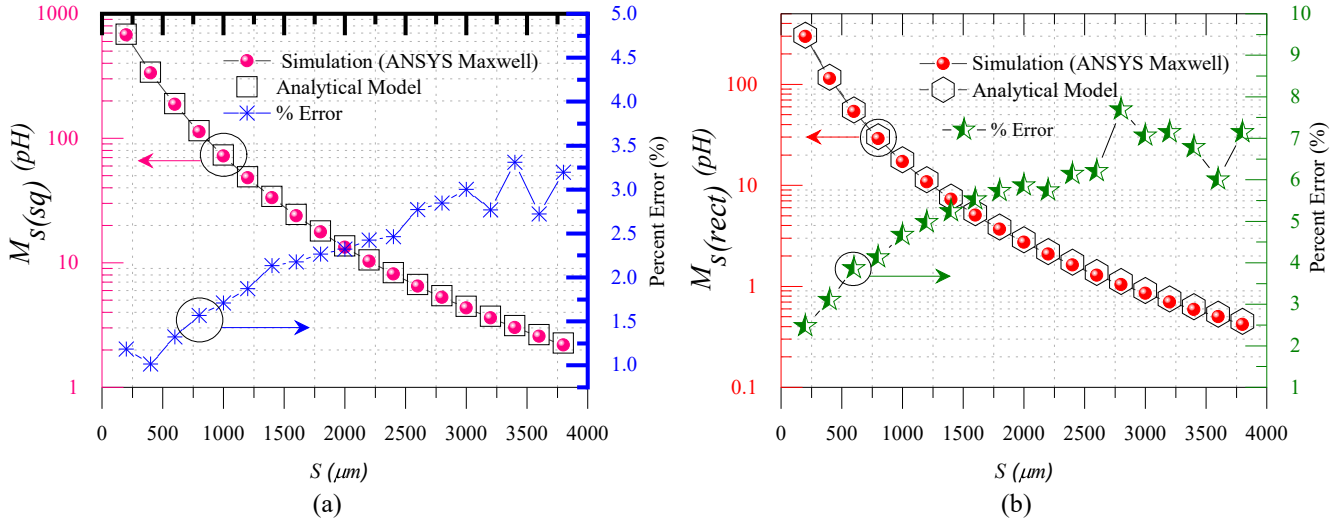

Fig. 12. Variation of mutual Inductance as a function of spacing, s, between the turns of *type 3*. (a) Square solenoid inductor ($1\ mm \times 1\ mm$). (b) Rectangular solenoid inductor ($0.5\ mm \times 1\ mm$).

the determination of the net mutual inductance needs the computation of mutual inductances between $6\times{}^{N}C_2$ pairs of conductors. However, in our model the calculation of the net mutual inductance requires only ${}^{N}C_2$ pairs of turns. Mutual inductance calculation of each pair, either turns or conductors, contributes certain amount of error. The greater the number of pairs, either turns or conductors, are employed for calculating mutual inductance, the more will be the error. Since our model demands less number of pair of turns than the number of pair of conductors, the model achieves higher accuracy. For the same reason, there is a drastic reduction in the simulation time of the proposed analytical model. The other two factors

This article has been accepted for publication in a future issue of this journal, but has not been fully edited. Content may change prior to final publication. Citation information: DOI 10.1109/JESTPE.2021.3077203, IEEE Journal of Emerging and Selected Topics in Power Electronics

TABLE VI
COMPARISON OF INDUCTANCE FROM OUR MODEL, CONVENTIONAL MODEL, SIMULATION (Q3D), AND MEASUREMENT OF EXAMPLE INDUCTOR FOR *TYPE 3*

N	**Width (mm)**	**Inductance (nH)**				**Percent Error (%)**			
		Our Model	Conventional Model (A.2)[2]	Q3D	Measurement@ frequency (MHz) [12]	Our Model versus		(A.2) versus	
						Q3D	[12]	Q3D	[12]
5	0.5	8.13	17.45	8.48	7.18@2	4.13	13.23	105.78	143.03
10	0.5	18.28	33.07	19.22	18.78 @2	4.89	2.66	72.06	43.21
15	0.5	28.60	48.75	30.31	29.62@2	5.64	3.44	60.84	39.24
20	0.5	38.98	64.44	41.40	39.16@2	5.85	0.46	55.65	39.23
5	1	16.68	34.91	16.98	15.65@1	1.77	6.58	105.59	55.17
10	1	39.61	66.14	40.52	35.38@1	2.25	11.96	63.23	46.50
15	1	63.37	97.5	65.04	58.73@1	2.57	7.90	49.91	39.76
20	1	87.37	128.89	89.74	75.17@1	2.64	16.23	43.63	41.67

[2] Refer to the Appendix A.

TABLE VII
COMPARISON OF INDUCTANCE FROM OUR MODEL, PUBLISHED MODEL, CONVENTIONAL MODEL, SIMULATION (Q3D), AND MEASUREMENT OF EXAMPLE INDUCTOR FOR *TYPE 4*

N	**Inductance (nH)**						**Percent Error (%)**				**Simulation Time (msec)**			
	Q3D		Analytical Model			(A.2)[a]	(Q3D vs Anal. Model)[b]			(A.2) vs Q3D[c]	Q3D (This work, [14], [15])	Our Model	Model [14]	Model [15]
	This Work	[14]& [15]	This Work	[14]	[15]		This Work	[14]	[15]					
1	0.589	0.60	0.586	0.53	0.59*	4.04	0.51	11.67	1.67	585.91	75	0.15[†]	14	20
2	1.67	1.69	1.65	1.55	1.64*	5.39	1.2	8.28	2.96	222.75	102		19	28
3	3.02	3.05	2.98	2.88	2.95*	7.28	1.32	5.57	3.28	141.06	172		21	32
4	4.54	4.59	4.48	4.43	4.44*	9.24	1.32	3.49	3.27	103.52	205		25	45
5	6.17	6.24	6.08	6.14	6.03*	11.24	1.46	1.60	3.37	82.17	268		27	49
6	7.88	7.97	7.76	7.85	7.7*	13.24	1.52	1.51	3.39	68.02	286		30	52
7	9.64	9.75	9.49	9.92	9.43*	15.25	1.56	1.75	3.28	58.20	314		32	53
8	11.44	11.58	11.26	11.95	11.19*	17.26	1.57	3.2	3.37	50.87	335		33	55
9	13.27	13.46	13.06	14.06	12.98*	19.28	1.58	4.46	3.57	45.29	365		35	56
10	15.14	15.34	14.87	16.22	14.79*	21.30	1.78	5.74	3.59	40.69	412		38	58

[*] Original values are corrected by deducting the contribution of the added extra term, i.e., internal inductance, to the expression (equation (3) from [15]) of the inductance of a rectangular cross section conductor.
[a] Conventional expression for the inductance of a solenoidal inductor (Refer to the Appendix A).
[b] This work, [14], and [15] analytical model results are compared with their corresponding Q3D results.
[c] Q3D results of this work.
[†] The maximum simulation time reported for running the MATLAB code for computing the inductance. The simulation time for all the turns approximately the same since the variation of the complexity of the code from 1 turn to 10 turns is not considerable.

TABLE VIII
COMPARISON OF INDUCTANCE FROM EXPRESSION AND SIMULATION FOR A RECTANGULAR CROSS SECTION CONDUCTOR

	Eq. (B.2) from this work[3] (224.73 pH)	Eq. (3) from [15] (239.73 pH)
Simulation (226.62 pH)	0.83%	5.79%

[3] Refer to the Appendix B.

contributing to the improvement of the simulation time can be explained as follows: (1) to calculate mutual inductance between any two turns, our model employs (C.10). On the other hand, model from [15] use (C.7), (C.8), and (C.9), which are complex and hence increase the simulation time. However, both models use (C.7)-(C.9) while computing the self-inductance of a single turn; (2) the code used to calculate the inductance has been optimized to reduce the simulation time.

Also, we have evaluated the accuracy of our model by comparing with measurement data for an inductor fabricated in-house. Our inductor has the following specifications: radius of the copper pillar ρ = 100 μm, length of the copper pillar l_p = 1530 μm, width of the interconnect α_i = 520 μm, height of the interconnect β_i = 35 μm, length of the top interconnect l_{ti} = 6100 μm, length of the bottom interconnect l_{bi} = 6130 μm, and the number of turns N is 6.25. The inductor was fabricated on a PCB; this does not detract the usefulness of the expression for the inductance since the effect of PCB substrate on the inductance in the frequency range of 1 to 100 MHz is insignificant provided that effects of parasitic capacitance is minimal. This is evident from Fig. 14, which is an experimental study. The high frequency effects are discussed in section VI. In Table IX, the inductance values from our model, conventional model, simulation, and our

This article has been accepted for publication in a future issue of this journal, but has not been fully edited. Content may change prior to final publication. Citation information: DOI 10.1109/JESTPE.2021.3077203, IEEE Journal of Emerging and Selected Topics in Power Electronics

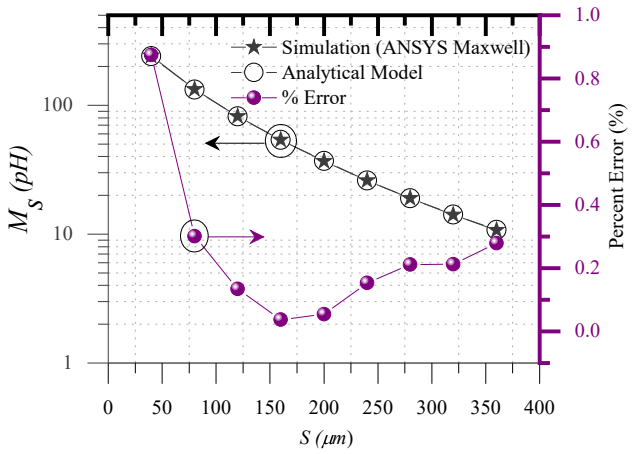

Fig. 13. Variation of mutual inductance as a function of spacing, s, between the turns of *type 4*.

measurement are compared.

TABLE IX
COMPARISON OF INDUCTANCE FROM OUR MODEL, CONVENTIONAL MODEL, SIMULATION, AND MEASUREMENT FOR *TYPE 4* PCB INDUCTOR

	Simulation (92.81 nH)	Our Measurement@0.5 MHz (89.60 nH)
Our Model (86.04 nH)	7.29%	3.97%
Conventional Model (A.2) (109 nH)	17.44%	21.65%

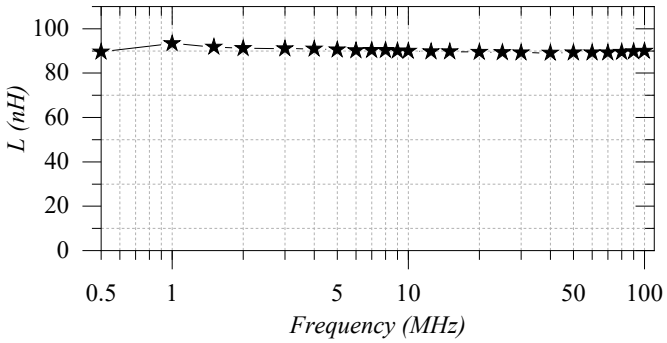

Fig. 14. Measured inductance as a function of frequency for the PCB inductor of *type 4*.

V. SIGNIFICANCE, APPLICATION AND PERFORMANCE

This section deals with significance, application and performance of all four types inductor structures. The available data from previously published works consolidated here to understand the importance of various types of inductor structures.

A. Significance and Application

The significance and applications of all four types of inductor structure given in Table X, which provides one application example from the literature for each of the four inductor types and describes the features that are specific to the inductor configurations.

B. Performance Comparison

We have presented performance data points for the various types of inductor structures in Table XI. The inductance density, DC resistance (DCR), and quality factor reported in the literature are reproduced. The published works have achieved a range of values of inductance, DCR and quality factor. We have presented only the optimum values achieved by them. For the *type 4* inductor, performance only at integrated power supply frequency (i.e., 100 MHz) is considered.

From Table XI, we can draw the following conclusions: (1) Solenoid inductors achieve higher inductance density compared to toroidal inductors, provided that dimensions of conductors and turn pitches of both types of inductors approximately remain same and (2) Inductors with smaller cross section conductors achieve high inductance density but low quality factor; the higher inductance density is due to low reluctance path and the lower quality factor is due to the increased resistance.

The published works presented in Table XI do not determine the required inductance values prior to the fabrication except in [13], where the maximum error between measured and estimated values is 11.42%. The proposed analytical models can provide a good initial estimation of inductance, which would help to achieve better figure of merit (FOM) values with minimal effort.

Finally, the summary of the performance of the proposed, conventional and published models are presented in Table XII.

VI. HIGH FREQUENCY EFFECTS ON INDUCTANCE

The self-inductance of each of the copper pillars and interconnects, which are building blocks of all four types of inductor structures, is the sum of internal inductance, L_{in}, and external inductance, L_{ex}. At very high frequency, the internal inductance vanishes due to skin effect (i.e., internal inductance approaches zero at a rate $\propto \frac{1}{\sqrt{f}}$)). On the other hand, external inductance remains the same as the total current in the conductor remains the same; this argument is strictly true for circular conductors but not for rectangular conductors, that is, $\Delta L_{ex} = 0$ for circular conductors and $\Delta L_{ex} \neq 0$ for rectangular conductors [27]. However, ΔL_{ex} can be considered as zero for rectangular conductors and in turn for the inductors in the frequency range of 1-100 MHz as the external H-field variation is not significant in the mentioned frequency range.

In this work, formula validations are performed for low frequencies or dc. For frequencies ranging from 1-100 MHz, the effect of skin effect on inductance is negligibly small. Consequently, the effect of higher frequencies (1-100 MHz) on total inductance is insignificant. The above explanation on the effect of frequency on air core inductance is consistent with the graph depicted in Fig. 15, which is the simulation study of the effect of frequency on inductance. An example inductor with even turns with specifications as given in Table I from [10] is considered for the study. It is evident from the Fig. 15 that the change in the inductance is only 0.47% from 1 to 100 MHz. The study considers only the skin effect and the capacitive coupling is ignored-in other words, the

TABLE X
SIGNIFICANCE AND APPLICATION OF ALL FOUR TYPES OF INDUCTOR STRUCTURES

Inductor Types	**Significance and Application**
Type 1	It was employed in a resonant converter at frequencies up to 33 MHz, resulting in a converter power density of $0.65W/cm^2$ [9]. The advantage is the mitigation of unintentional coupling due to the confinement of magnetic flux to a circular region.
Type 2	Similar to the *type 1*, this inductor also offers the advantages such as low EMI and reduced eddy current loss. As far as the fabrication is concerned, this type helps in reducing overall processing time as explained in section III. The inductor structure finds application in ultra-compact DC-DC converters [11], [25]
Type 3	Exhibits high inductance density compared to *type 1* and *type 2*. Hence, it can be an excellent candidate for integrating into power MEMS devices [12].
Type 4	The inductance density is on a par with *type 3*. This type of inductor architecture was developed for hybrid IC applications [13]. It has been applied to produce inductors in the range of 0.88-4.66nH for operation at 100 MHz.

TABLE XI
COMPARISON OF THE MEASURED INDUCTANCE, DCR AND QUALITY FACTOR OF VARIOUS EXAMPLES OF INDUCTOR TYPES

Reported Work	Type	$L_{density}$ (nH/mm^3)	DCR (mΩ)	Q@frequency (MHz)
[10]	*Type 1*	17.3	180	12.9@41.2
[25]	*Type 2*	4.16	400	17.5@70
[12]	*Type 3*	21.7	NA‡‡	37.6@21
[13]	*Type 4*	44.53	NA‡‡	6.78@100

‡‡ Not Available.

TABLE XII
COMPARISON OF OUR MODEL, CONVENTIONAL MODEL, AND PUBLISHED MODEL OF ALL FOUR TYPES OF INDUCTORS

Inductor Types	**Maximum Percent Error (%)** (Comparison with FEA Solution)		
	Our Model	Conventional Model‡	Published Model
Type 1	5.79	46.33	NA**
Type 2	6.78	32.87	NA**
Type 3	5.85	105.78	NA**
Type 4	1.78	585.91	11.67 [14] & 3.59 [15]

‡ Conventional expressions for the inductance of solenodal and toroidal inductors are given in Appendix A.
** Not available

simulation does not consider the effect of parasitic capacitance. The parasitic capacitance model of toroid air core inductors presented in [28] composed of the following components: the capacitance between adjacent turns, the capacitance between the inner and outer copper pillars of the same turn, and the capacitance between the top and bottom interconnects of the same turn. In this model, the capacitance between non-adjacent turns is neglected. Similarly, the parasitic capacitance model of a solenoid inductor is discussed in [12].

The effect of frequency on air core and silicon core inductors is illustrated in [10, Fig. 7(d)], which is the measured inductance characteristics of the inductor with even number of turns; the specifications of the inductor are given in Table I. The drop in the inductances over 1 to 100 MHz for the air core and silicon core inductors are 5.21% and 12.94%, respectively. The drop in the inductance for air core inductor is mainly due to parasitic capacitance, whereas for silicon core inductor its due to parasitic capacitance as well as eddy current. The percentage change in the inductance over the frequency range of interest is high in the case of silicon core inductors due to large parasitic capacitance, $3\times$ higher than air core inductor capacitance. The larger turn spacing, s, reduces capacitive coupling and hence the drop in the inductance is smaller. This statement can be supported by Fig. 14 which shows the measured inductance values for the PCB inductor over the frequency range from 1 to 100 MHz. The percentage change in the inductance over the given frequency range is only 3.74%, less than both silicon core and air core inductors, attributed to larger turn spacing of the PCB inductor.

In conclusion, we can safely ignore the effects of high frequency (1-100 MHz) on the inductance and hence the analytical model of dc inductance can be adapted without any appreciable error provided that parasitic capacitances and eddy currents are minimal.

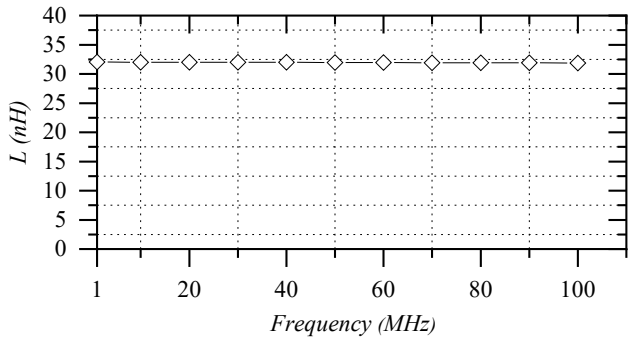

Fig. 15. Plot showing inductance from FEM simulation versus frequency.

VII. Conclusion

This work focused on analytical research. An accurate analytical method provides guidance in research planning. Unlike experimental research, the analytical method can be applied over a wide range of conditions, which will save money, time and, human resources.

We have presented the analytical models for the inductances of four types of 3D inductor structures. To ease the analytical modelling process, the physical structures of these inductors are modified: 3D inductors are conceptualized as a group of loop currents or piecewise current sources. This enables us to use the concept of the partial and loop inductances to determine the inductances of all the four types of inductors.

This article has been accepted for publication in a future issue of this journal, but has not been fully edited. Content may change prior to final publication. Citation information: DOI 10.1109/JESTPE.2021.3077203, IEEE Journal of Emerging and Selected Topics in Power Electronics

We derived equations relating the partial and loop inductances (self and mutual) to the inductances of all the four inductor formats. All the proposed models are tested with fabricated inductors: the first three types are tested with the fabricated inductors from previously published works and the last type is tested with an inductor fabricated in-house. The proposed analytical model result of the *type 1* inductor is in good agreement with field solver result ($<$ 5.8% error). The measurement data [25] is in close agreement with the analytical expression result for the *type 2* inductor, error is about 1.5%, while the comparison of the model result of the *type 2* with FEA simulation demonstrates an error of 6.78%. An effort has been made to keep analytical model of *type 3* inductor as simple as possible while maintaining good accuracy ($<$ 5.9% error), by comparison with simulation; also, the correlation between model and measurement [12] exhibits errors ranging from 0.46-16.23%. For the *type 4* inductor, our analytical model reduces the error, when correlated with FEA inductance value, by up to $6\times$ and $2\times$ compared to the previously published models [14], [15], respectively. The error between the analytical model result and the previously published measurement data is as high as 16.09% for *type 1* inductor and 16.23% for *type 3* inductor. This is due to the following reasons: (1) geometrical difference between the modelled and fabricated inductors and (2) experimental set up under which the inductance was measured.

The comparison results verify that as the size of the inductor decreases the error introduced by conventional models will rise dramatically. This indicates that conventional expressions for the inductance are not suitable for micro fabricated inductors. From the experimental and simulation study of this work as well as experimental data [10, Fig. 7(d)], the effect of high frequency (1-100 MHz) on the inductance of air core inductor or silicon core inductor or PCB inductor can be neglected provided that the parasitic capacitances and eddy currents are minimal and the analytical model of dc inductance can be adapted without significant error. The proposed analytical models can be employed for calculating the inductance of 3D air core, 3D silicon core, and PCB air core inductors in the frequency range of 1 to 100 MHz. The results of the proposed models could serve as a good initial estimate even if there are minor geometrical differences between modelled and fabricated inductors.

APPENDIX A
CONVENTIONAL FORMULAE

Conventional formulas, given by (A.1) [28]–[30] and (A.2), are reproduced here. Equations (A.1) and (A.2) are conventional models for the inductance of toroidal and solenoidal inductors, respectively.

$$L = \frac{N^2 h \mu_o}{2\pi} ln\left(\frac{R_o}{R_i}\right) + \left(\frac{R_o + R_i}{2}\right)\mu_o \times \left[\ln\left(8 \times \frac{R_o + R_i}{R_o - R_i}\right) - 2\right] \quad \text{(A.1)}$$

$$L = \frac{\mu_o N^2 A}{l} \quad \text{(A.2)}$$

where h, R_i and R_o are the height, inner radius, and outer radius of the toroidal inductor, respectively, l and A are the length and area of the solenoid inductor, respectively, and N is the number of turns.

The first term of (A.1) is the inductance due to the magnetic energy stored inside the toroid and the second term is due to the circumferential current, which appears only at high frequency. The second term is generally referred to as single-turn inductance: the toroid is treated as a circular loop of conducting wire to derive the second term. The formula for the inductance of a circular loop is given in [31]. If we substitute loop radius as $0.5(R_o+R_i)$ and wire radius as $0.5(R_o-R_i)$ in the inductance formula for a circular loop, we get the second term of (A.1).

APPENDIX B
SELF-INDUCTANCE FORMULAE

$$L_{circ}(l,\rho) = \frac{\mu_o}{2\pi}\left[l\ ln\left(\frac{l+\sqrt{l^2+\rho^2}}{\rho}\right) - \sqrt{l^2+\rho^2} + \frac{l}{4} + \rho\right] \quad \text{(B.1)}$$

$$L_{rect}(l,\alpha,\beta) = \frac{\mu_o\ l}{2\pi}\left[ln\left(\frac{2l}{\alpha+\beta}\right) + 0.5 + \frac{\alpha+\beta}{3l}\right] \quad \text{(B.2)}$$

$$L_{sq\_1}(a,\alpha,\beta) = \frac{\mu_o}{2\pi}\left(4a\left(\ln\left(\frac{a}{\alpha+\beta}\right) + 0.2235\left(\frac{\alpha+\beta}{a}\right) + 0.726\right)\right) \quad \text{(B.5)}$$

$$L_{sq\_2}(a,\alpha) = \frac{\mu_o}{2\pi}\left(4a\left[\ln\left(\frac{a}{\alpha}\right) + 0.447\left(\frac{\alpha}{a}\right) + 0.033\right]\right) \quad \text{(B.6)}$$

APPENDIX C
MUTUAL INDUCTANCE FORMULAE

$$M_{par}(l,D) = \frac{\mu_o}{2\pi}\left[l\ ln\left(\frac{l+\sqrt{l^2+D^2}}{D}\right) - \sqrt{l^2+D^2} + D\right] \quad \text{(C.1)}$$

$$M_{lm\_1}(l,m,\mu,\nu,\theta) = \frac{\mu_o}{2\pi}\left(cos\theta\left[(\mu+l)\tanh^{-1}\left(\frac{m}{r_1+r_2}\right) + (\nu+m)\tanh^{-1}\left(\frac{l}{r_1+r_4}\right) - \mu\ tanh^{-1}\left(\frac{m}{r_3+r_4}\right) - \nu\ tanh^{-1}\left(\frac{l}{r_2+r_3}\right)\right]\right) \quad \text{(C.2)}$$

This article has been accepted for publication in a future issue of this journal, but has not been fully edited. Content may change prior to final publication. Citation information: DOI 10.1109/JESTPE.2021.3077203, IEEE Journal of Emerging and Selected Topics in Power Electronics

$$L_{RECT\_1}(a,b,\alpha_a,\beta_a,\alpha_b,\beta_b) = \frac{\mu_o}{2\pi}\left(2\left(a\ ln\left(\frac{2ab}{\alpha_a+\beta_a}\right) - a\ ln\left(a+z\right) + 0.5a - b + z + 0.2235(\alpha_a+\beta_a)\right)\right.$$
$$\left. +2\left(b\ ln\left(\frac{2ab}{\alpha_b+\beta_b}\right) - b\ ln\left(b+z\right) + 0.5b - a + z + 0.2235(\alpha_b+\beta_b)\right)\right) \quad \text{(B.3)}$$

where z is the diagonal of the rectangle, which is equal to: $z = \sqrt{a^2+b^2}$.

$$L_{RECT\_2}(a,b,\alpha,\beta) = \frac{\mu_o}{2\pi}\left(2\left((a+b)\ \ln\left(\frac{2ab}{\alpha+\beta}\right) - a\ \ln\left(a+z\right) - b\ \ln\left(b+z\right) - \left(\frac{a+b}{2}\right) + 2z + 0.447(\alpha+\beta)\right)\right) \quad \text{(B.4)}$$

$$r_1(l,m,\mu,\nu,\theta) = \left(\left(\mu+l\right)^2 + \left(\nu+m\right)^2 - 2\left(\mu+l\right)\left(\nu+m\right)cos\theta\right)^{1/2} \quad \text{(C.3)}$$

$$r_2(l,\mu,\nu,\theta) = \sqrt{\left(\mu+l\right)^2 + \nu^2 - 2\nu\left(\mu+l\right)cos\theta} \quad \text{(C.4)}$$

$$r_3(\mu,\nu,\theta) = \sqrt{\mu^2+\nu^2-2\mu\nu\cos\theta} \quad \text{(C.5)}$$

$$r_4(m,\mu,\nu,\theta) = \sqrt{\mu^2 + \left(\nu+m\right)^2 - 2\mu\left(\nu+m\right)cos\theta} \quad \text{(C.6)}$$

$$R_i = \sum_{i=1}^{4}\sqrt{d^2+{r_i}^2} \quad \text{(C.7)}$$

$$M_{lm\_2}(l,m,d,\mu,\nu,\theta) = \frac{\mu_o}{2\pi}\left(cos\theta\left[\left(\mu+l\right)tanh^{-1}\left(\frac{m}{R_1+R_2}\right) + \left(\nu+m\right)tanh^{-1}\left(\frac{l}{R_1+R_4}\right) - \mu\ tanh^{-1}\left(\frac{m}{R_3+R_4}\right) - \nu\ tanh^{-1}\left(\frac{l}{R_2+R_3}\right)\right] - \frac{\Omega d}{2\ tan\theta}\right) \quad \text{(C.8)}$$

$$\Omega(l,m,d,\mu,\nu,\theta) = tan^{-1}\left\{\frac{d^2cos\theta\ + \left(\mu+l\right)\left(\nu+m\right)sin^2\theta}{dR_1sin\theta}\right\} - tan^{-1}\left\{\frac{d^2cos\theta\ + \left(\mu+l\right)\nu sin^2\theta}{dR_2sin\theta}\right\} - tan^{-1}\left\{\frac{d^2cos\theta\ + \mu\left(\nu+m\right)sin^2\theta}{dR_4sin\theta}\right\} + tan^{-1}\left\{\frac{d^2cos\theta\ + \mu\nu sin^2\theta}{dR_3sin\theta}\right\} \quad \text{(C.9)}$$

$$M_{rect}(a,b,s) = \frac{\mu_o}{2\pi}\left(2\left(a\ ln\left(\frac{a+\sqrt{a^2+s^2}}{a+\sqrt{a^2+b^2+s^2}}\frac{\sqrt{b^2+s^2}}{s}\right) + b\ ln\left(\frac{b+\sqrt{b^2+s^2}}{b+\sqrt{a^2+b^2+s^2}}\frac{\sqrt{a^2+s^2}}{s}\right)\right) + 4\left(\sqrt{a^2+b^2+s^2} - \sqrt{a^2+s^2} - \sqrt{b^2+s^2} + s\right)\right) \quad \text{(C.10)}$$

$$M_{sq}(a,s) = \frac{\mu_o}{2\pi}\left(4\left[a\ ln\left(\frac{a+\sqrt{a^2+s^2}}{a+\sqrt{2a^2+s^2}}\frac{\sqrt{a^2+s^2}}{s}\right)\right] + 4\left[\sqrt{2a^2+s^2} - 2\sqrt{a^2+s^2} + s\right]\right) \quad \text{(C.11)}$$

ACKNOWLEDGMENT

This work was conducted at Tyndall National Institute, Ireland and National University of Ireland Galway.

REFERENCES

[1] C. . Mathúna, N. Wang, S. Kulkarni, and S. Roy, "Review of integrated magnetics for power supply on chip (PwrSoc)," *IEEE Transactions on Power Electronics*, vol. 27, no. 11, pp. 4799–4816, Nov 2012.

[2] X. Sun, G. Van der Plas, and E. Beyne, "Improved staggered through silicon via inductors for RF and power applications," in *Proc. IEEE 68th Electronic Components and Technology Conference (ECTC)*, 2018, pp. 1692–1697.

[3] H. T. Le, Y. Nour, Z. Pavlovic, C. O'Mathúna, A. Knott, F. Jensen, A. Han, S. Kulkarni, and Z. Ouyang, "High-Q Three-dimensional microfabricated magnetic-core toroidal inductors for power supplies in package," *IEEE Transactions on Power Electronics*, vol. 34, no. 1, pp. 74–85, Jan 2019.

[4] S. Kulkarni, D. Li, D. Jordan, N. Wang, and C. Ó Mathúna, "PCB embedded bondwire inductors with discrete thin-film magnetic core for power supply in package," *IEEE Journal of Emerging and Selected Topics in Power Electronics*, vol. 6, no. 2, pp. 614–620, June 2018.

[5] J. Kim, J.-K. Kim, M. Kim, F. Herrault, and M. G. Allen, "Microfabrication of toroidal inductors integrated with nanolaminated ferromagnetic metallic cores," *Journal of Micromechanics and Microengineering*, vol. 23, no. 11, p. 114006, oct 2013.

[6] W. Liang, L. Raymond, and J. Rivas, "3-D-printed air-core inductors for high-frequency power converters," *IEEE Transactions on Power Electronics*, vol. 31, no. 1, pp. 52–64, Jan 2016.

[7] R. Meere, N. Wang, T. O'Donnell, S. Kulkarni, S. Roy, and S. C. O'Mathuna, "Magnetic-core and air-core inductors on silicon: A performance comparison up to 100 MHz," *IEEE Transactions on Magnetics*, vol. 47, no. 10, pp. 4429–4432, Oct 2011.

[8] C. R. Sullivan, "Integrating magnetics for on-chip power: Challenges and opportunities," in *Proc. IEEE Custom Integrated Circuits Conference*, 2009, pp. 291–298.

[9] H. Thanh Le, Y. Nour, A. Han, F. Jensen, Z. Ouyang, and A. Knott, "Microfabricated air-core toroidal inductor in very high-frequency power converters," *IEEE Journal of Emerging and Selected Topics in Power Electronics*, vol. 6, no. 2, pp. 604–613, June 2018.

[10] H. T. Le, I. Mizushima, Y. Nour, P. T. Tang, A. Knott, Z. Ouyang, F. Jensen, and A. Han, "Fabrication of 3D air-core MEMS inductors for very-high-frequency power conversions," *Microsystems & Nanoengineering*, vol. 4, no. 1, pp. 1–9, Jan 2018.

[11] X. Yu, M. Kim, F. Herrault, C. Ji, J. Kim, and M. G. Allen, "Silicon-embedded 3D toroidal air-core inductor with through-wafer interconnect for on-chip integration," in *Proc. IEEE 25th International Conference on Micro Electro Mechanical Systems (MEMS)*, 2012, pp. 325–328.

[12] T. Xu, J. Sun, H. Wu, H. Li, H. Li, and Z. Tao, "3D MEMS in-chip solenoid inductor with high inductance density for power MEMS device," *IEEE Electron Device Letters*, vol. 40, no. 11, pp. 1816–1819, Nov 2019.

[13] M. Duplessis, O. Tesson, F. Neuilly, J. R. Tenailleau, and P. Descamps, "Physical implementation of 3D integrated solenoids within silicon substrate for hybrid IC applications," in *Proc. European Microwave Conference (EuMC)*, 2009, pp. 1006–1009.

[14] F. Wang and N. Yu, "Simple and accurate inductance model of 3D inductor based on TSV," *Electronics Letters*, vol. 52, no. 21, pp. 1815–1816, Oct. 2016.

[15] S. Gou, G. Dong, Z. Mei, and Y. Yang, "Accurate inductance modeling of 3-D inductor based on TSV," *IEEE Microwave and Wireless Components Letters*, vol. 28, no. 10, pp. 900–902, Oct 2018.

[16] E. B. Rosa, "The self and mutual inductances of linear conductors," *Bulletin of Bureau of Standards*, vol. 4, no. 2, pp. 301–344, Sep 1907.

[17] F. W. Grover, *Inductance Calculations*. New York: Dover Publications, 1973, pp. 55–58.

[18] C. R. Paul, *Inductance: Loop and Partial*. New York, USA: Wiley, 2010, pp. 236–239.

[19] H. Greenhouse, "Design of planar rectangular microelectronic inductors," *IEEE Transactions on Parts, Hybrids, and Packaging*, vol. 10, no. 2, pp. 101–109, June 1974.

[20] C. R. Paul, *The Concept of Partial Inductance*. USA: Wiley-IEEE Press, 2010, pp. 195–245.

[21] I. P. Vaisband, R. Jakushokas, M. Popovich, A. V. Mezhiba, S. Köse, and E. G. Friedman, *On-chip power delivery and management*. Switzerland: Springer, 2016, pp. 31–35.

[22] J. Kim, F. Herrault, X. Yu, M. Kim, R. H. Shafer, and M. G. Allen, "Microfabrication of air core power inductors with metal-encapsulated polymer vias," *Journal of Micromechanics and Microengineering*, vol. 23, no. 3, pp. 1–7, jan 2013.

[23] U. R. Tida, R. Yang, C. Zhuo, and Y. Shi, "On the efficacy of Through-Silicon-Via inductors," *IEEE Transactions on Very Large Scale Integration (VLSI) Systems*, vol. 23, no. 7, pp. 1322–1334, July 2015.

[24] S. Mondal, S. Cho, and B. C. Kim, "Modeling and crosstalk evaluation of 3-D TSV-based inductor with ground TSV shielding," *IEEE Transactions on Very Large Scale Integration (VLSI) Systems*, vol. 25, no. 1, pp. 308–318, Jan 2017.

[25] X. Yu, M. Kim, F. Herrault, C. Ji, J. Kim, and M. G. Allen, "Silicon-embedding approaches to 3-D toroidal inductor fabrication," *Journal of Microelectromechanical Systems*, vol. 22, no. 3, pp. 580–588, June 2013.

[26] G. Burger, E. Smulders, J. Berenschot, T. Lammerink, J. Fluitman, and S. Imai, "High-resolution shadow-mask patterning in deep holes and its application to an electrical wafer feed-through," *Sensors and Actuators A: Physical*, vol. 54, no. 1, pp. 669 – 673, June 1996.

[27] C. L. Holloway, E. F. Kuester, A. E. Ruehli, and G. Antonini, "Partial and internal inductance: Two of Clayton R. Paul's many passions," *IEEE Transactions on Electromagnetic Compatibility*, vol. 55, no. 4, pp. 600–613, Aug 2013.

[28] C. R. Sullivan, W. Li, S. Prabhakaran, and S. Lu, "Design and fabrication of low-loss toroidal air-core inductors," in *Proc. IEEE Power Electronics Specialists Conference*, 2007, pp. 1754–1759.

[29] G. Zulauf, W. Liang, and J. Rivas-Davila, "A unified model for high-power, air-core toroidal PCB inductors," in *Proc. IEEE 18th Workshop on Control and Modeling for Power Electronics (COMPEL)*, 2017, pp. 1–8.

[30] J. Qiu, D. V. Harburg, and C. R. Sullivan, "A toroidal power inductor using radial-anisotropy thin-film magnetic material based on a hybrid fabrication process," in *Proc. Twenty-Eighth Annual IEEE Applied Power Electronics Conference and Exposition (APEC)*, 2013, pp. 1660–1667.

[31] C. R. Paul, *Inductance: Loop and Partial*. New York, USA: Wiley, 2010, pp. 126–130.